Journal of Renewable and Sustainable Energy

RESEARCH ARTICLE | SEPTEMBER 25 2024

A multi-decadal analysis of U.S. and Canadian wind and solar energy droughts

James M. Wilczak ; Elena Akish ; Antonietta Capotondi; Gilbert P. Compo ; Andrew Hoell

J. Renewable Sustainable Energy 16, 056502 (2024)
https://doi.org/10.1063/5.0219648

Journal of Renewable and Sustainable Energy ARTICLE pubs.aip.org/aip/rse

A multi-decadal analysis of U.S. and Canadian wind and solar energy droughts

Cite as: J. Renewable Sustainable Energy **16**, 056502 (2024); doi: 10.1063/5.0219648
Submitted: 18 May 2024 · Accepted: 29 August 2024 ·
Published Online: 25 September 2024

View Online Export Citation CrossMark

James M. Wilczak,[1,a] Elena Akish,[1,2,b] Antonietta Capotondi,[1,2,c] Gilbert P. Compo,[1,2,d] and Andrew Hoell[1,e]

AFFILIATIONS

[1]NOAA Physical Sciences Laboratory, Boulder, Colorado 80305, USA
[2]Cooperative Institute for Research in Environmental Sciences (CIRES), University of Colorado, Boulder, Colorado 80309, USA

[a]Author to whom correspondence should be addressed: james.m.wilczak@noaa.gov
[b]Electronic mail: akishelena@gmail.com
[c]Electronic mail: antonietta.capotondi@noaa.gov
[d]Electronic mail: gilbert.p.compo@noaa.gov
[e]Electronic mail: andrew.hoell@noaa.gov

ABSTRACT

The spatial and temporal characteristics of wind and solar energy droughts across the contiguous U.S. and most of Canada for the period 1959–2022 are investigated using bias-corrected values of daily wind and solar power generation derived from the ERA5 meteorological reanalysis. The analysis domain has been divided into regions that correspond to four major interconnects and nine sub-regions. Droughts are examined for wind alone, solar alone, or a mix of wind and solar in which each provides 50% of the long-term mean energy produced, for durations of 1–90 days. Wind and solar energy droughts and floods are characterized on a regional basis through intensity–duration–frequency curves. Wind and solar generation are shown to be weakly anti-correlated over most of the analysis domain, with the exception of the southwest U.S. The intensities of wind and solar droughts are found to be strongly dependent on region. In addition, the wind resource in the central U.S. and the solar resource in the southwestern U.S. are sufficiently good that over-weighting capacity in those areas would help mitigate droughts that span the contiguous United States for most duration lengths. The correlation of droughts for the 50%–50% mix of wind and solar generation with temperature shows that the most intense droughts occur when temperatures exhibit relatively moderate values, not when energy demand will be largest. Finally, for all regions except the southeast U.S., winter droughts will have a larger impact on balancing the electric grid than summer droughts.

I. INTRODUCTION

As countries begin to develop low-carbon energy systems based on electrification of energy use that include significant renewable energy generation, a central issue is how to design these systems to account for the variability of wind and solar generation. Because electricity demand must always be met with supply, the design of such future energy systems must consider the most extreme low wind and solar generation events, especially those that occur concurrently with periods of high energy demand.

When periods of anomalously low wind energy production or solar energy production persist in time and cover large geographic areas, they are commonly referred to as wind and solar energy droughts. Knowledge of the characteristics of these energy droughts will be essential for determining the design and operation of a future electric energy system in which wind and solar generation are major contributors, and for determining the roles of transmission, overbuilding of generation, longer-term energy storage, and demand response. In this study, we attempt to provide some insights into the nature of wind and solar energy droughts across the contiguous U.S. and Canada through the use of wind speed and solar irradiance estimates derived from a bias-corrected version of the multi-decadal ERA5 reanalysis dataset.[1]

The minimum duration of a consequential wind or solar energy system drought will depend on the ability of the energy system to smooth over short-term fluctuations in wind and solar energy supply. Many new renewable energy plants are being built as hybrid solar and battery, or wind and battery combinations, with the batteries, when fully charged, able to provide several hours of equivalent power output. Electric vehicles may also offer the possibility of providing short-term grid balancing by returning electricity to the grid. Therefore, we

assume that for all balancing areas a combination of battery, demand response, or other mechanisms will be sufficient to match the diurnal variation of load and supply for a climatologically average weather day, shifting excess production in some hours of the day to other hours with a shortfall of production. Wind and solar energy droughts in our analysis therefore span time scales from a minimum duration of one day, out to weeks, months, and seasons. Wind and solar energy droughts can be impactful on time scales as short as even 1-day because wind and solar power have no natural storage, equivalent to soil moisture or snow pack for hydrologic droughts.

This study is complementary to recent grid-integration studies[2–6] that have investigated renewable energy variability and grid balancing issues over relatively short multi-year timescales (often using 3–7 years of weather data). Most of these studies have used complex capacity expansion models including transmission, storage, weather dependent generation, and estimates of future generation costs and electricity demand to find the optimal, lowest cost configuration of wind and solar plants and transmission that will provide a reliable power system. The optimal solution strongly depends on the weather, and in particular, on the characteristics of periods of low wind and solar energy production. However, these studies have primarily focused on determining whether, and at what cost, electrical energy demand and supply can be balanced at each moment in time using a combination of renewable and fossil fuel generation, transmission, and storage, with little description of the meteorology involved. In contrast, our goal in the current study is to provide a detailed spatial and temporal meteorological characterization of wind and solar droughts that have occurred over past decades and to highlight the challenges they present to the reliability of a highly renewables-based energy system.

Specific questions to be answered are:

(1) Are there meaningful trends in the mean wind and solar resources relative to their variability in the ERA5 dataset over the U.S. and Canada?
(2) How significant can wind and solar droughts be?
(3) What are the spatial and temporal characteristics of wind and solar energy droughts? How do they vary geographically, and by season?
(4) Do wind and solar droughts act in phase or out of phase with one another, and is this correlation geographically dependent?
(5) Are wind and solar droughts correlated with temperature (energy demand) extremes?

II. WIND AND SOLAR ENERGY GENERATION DROUGHT DEFINITION

Identifying an optimal definition of water-related droughts has long challenged scientists, both because of the complexity of the hydrologic system and because the utility of a definition will depend on the particular application it will address. Consequently, numerous approaches and definitions have been proposed, and for many users, value is found in using multiple drought definitions. It should not be surprising then, that a renewable energy drought definition will be equally enigmatic and multi-faceted. For any renewable energy drought definition, however, several characteristics are desired: (1) it should quantify how little energy has been produced over varying time and spatial scales; (2) it should allow a comparison of wind, solar, or hydropower droughts across regions; (3) it should be independent of *ad hoc* thresholds that are not derived from power system attributes; and (4) it should provide a basis for understanding the results of grid-integration studies, especially those using complex capacity expansion models that provide detailed prescriptions of where and how much wind and solar generation, storage, and transmission will be needed in a future energy system.

Following Raynaud *et al.*,[7] it is common to classify renewable energy droughts either as generation shortfalls relative to a generation metric, or as net energy balance shortfalls that consider the difference between generation and demand. Generation droughts can be further separated into those that determine the shortfalls relative to a seasonally varying mean production, or those that include the seasonal variation of generation by calculating the shortfalls relative to the long-term mean production. Because the grid must be balanced including those seasonal variations, from an energy systems perspective we believe it is more useful to calculate wind and solar power anomalies including those seasonal variations, i.e., relative to the annual mean. Net energy balance shortfall methods generally have included the seasonal variations of generation and demand by calculating droughts as periods when generation is less than demand, independent of season. Although we include the seasonal cycles of generation in our drought definition, in Sec. VIII we also quantify separately the contributions to droughts from short-term weather and interannual climate variations and those from the mean seasonal cycles of generation.

Energy generation and energy supply droughts can be divided into those that first apply criteria to intensity and then find the resulting durations, or those that first apply criteria to duration and then find the resulting intensities. Using the terminology introduced by Patlakas *et al.*,[8] we refer to these two categories of methodologies as Duration Given Intensity (DGI) and Intensity Given Duration (IGD). The DGI approach determines the durations of the worst droughts above a given intensity threshold, while the IGD approach determines the intensities of the worst droughts for a given duration. From both the DGI and IGD methods, intensity–duration–frequency (IDF) curves can be derived, which is a part of the analysis of many, but not all of the previous studies in this area. Most of the literature on renewable energy droughts has focused on the DGI approach. Typically, a single fixed, or small set of drought intensity threshold values are selected, and periods of drought are identified as those times when the drought surpasses the intensity threshold. Drought intensity is often defined as a fixed capacity factor (CF) value,[9–16] where CF is the ratio of actual energy output over a given period of time to the theoretical maximum energy output possible. Other definitions consider a fixed percent of the long-term mean production[7,17–20] a long-term day of year production,[21] a fixed wind speed value,[22–24] a percent of the maximum generation value,[25] or a fixed standardized index value[26,27] which incorporates the standard deviation of the generation. A variant of the above methods is one in which a continuum of intensity thresholds is applied.[28] A drawback of the DGI methods that use fixed thresholds is that the thresholds do not derive from any attribute of the energy system, but are *ad hoc* subjective choices.

Although commonly used for water-related droughts, the IGD approach has been used less often than the DGI approach for renewable energy droughts. Brown *et al.*[29] use a single duration of 1 week, and then classify a week as being in drought if the weekly mean value exceeds a mean power percent threshold. Rinaldi *et al.*[30] use a set of four duration values, then also use a power threshold set to a percent

of the mean production. Ohba *et al.*[31] use three fixed durations of 1, 3, and 5 days, and then set a threshold CF. A drawback of approaches that apply fixed intensity threshold values to fixed duration events is that again neither of these parameters derive from any attribute of the energy system. Leahy and McKeogh[32] select a fixed set of duration lengths, find the worst drought in each year of their dataset, fit a generalized extreme value (GEV) curve to those values, and then calculate return periods based on the GEV fits. This has the advantage that no arbitrary intensity thresholds are imposed to define a drought, although a pre-determined set of durations is chosen. Patlakas *et al.*[8] take a similar approach, but use a continuum of durations by applying moving averages whose window length increments by steps equal to the time-resolution of the data used, and then find GEV fits to the probability density functions, from which IDF curves spanning all durations are derived. Ruhnau and Qvist[33] start with a time series of energy deficits relative to demand, calculate integrated deficit values over a continuum of durations, and then find the duration value at which the integrated deficit reaches a maximum, for which the storage capacity needed would also be its maximum value. This period of maximum energy deficit is commensurate with the worst energy supply drought. As their study focuses on the energy storage requirements to mitigate that worst-case drought, they do not further explore the characteristics of drought events. (Note that their integral method is equivalent to finding the largest negative anomaly of a series of moving averages).

This study considers energy generation droughts, independent of energy demand, and it includes seasonal variations of generation when calculating those droughts. In order to more readily compare drought anomaly events between different geographic regions, CFs are converted into normalized power by dividing each day's CF by the long-term mean CF for each region, and then multiplying by 100 to get a percent. The power produced during drought events then ranges from 0% to 100%, while the power produced during floods will be any value greater than 100%. For locations with small mean CFs it is possible for the flood anomalies to be quite large. For example, a region that is almost always cloudy will have a small solar CF value, but on a rare sunny day the normalized power may reach several multiples of 100%.

In addition, this study takes an approach similar to Patlakas *et al.*[8] and Ruhnau and Qvist[33] in that it uses a continuum of duration lengths, applying moving means of lengths 1–90 days to daily time series of wind, solar, or a mix of wind and solar normalized power. Here the running mean length is equivalent to the duration of each drought event. The minimum value from each of these 90 timeseries is then found over the entire period of record, and these are plotted as a curve of drought intensity vs duration, depicting the single worst drought at each duration value. Next, for the running mean = 1 time series, the worst drought is removed from the time series, and the second worst event is found. This procedure is repeated up to N times, where N signifies the number of drought events found, i.e., the first, second, third, … Nth worst drought events. The same N-step process is then applied starting with the complete running mean = 2 time series, removing the 2 days that comprise the worst 2-day anomaly, and repeating up to N times. The entire process is repeated for running means out to duration = 90 days. Empirical return periods are estimated for each of the N steps according to the Weibull formula

$$T = \frac{n+1}{m},$$

where n is the number of years of data, m is the rank of the event (m = 1, N), and T is the return period in years. In the present analysis, n = 64 years and IDF curves are calculated for N = 16 values, which are then displayed for m = 1, 4, and 16, corresponding to return periods of approximately 65, 16, and 4 years. We call this the continuous drought duration-return period (CDD-RP) method.

In the above drought identification procedure, each time that an event is removed, it is equivalent to setting an intensity threshold at the level of the latest event removed. For each duration, the implicit intensity threshold of the Nth event removed will vary, and will become smaller at longer durations. Unlike methods that impose *ad hoc* intensity thresholds that are not linked to any energy system attribute, the proposed method selects a desired return period, which is an energy system attribute based on the tolerance of the grid (or society) to accept these shortages and mitigate them through energy storage, demand response, or load shedding, and then implicitly finds the corresponding intensity threshold needed for that return period.

Also, it is noted that each of the N drought events at each duration value are independent, non-overlapping events. However, as the event selection is done independently for each duration, droughts for adjacent durations can and will select similar days for their respective N worst droughts. This is no different than analyses of precipitation floods based on fixed durations of say, 1, 6, and 12 h, where the time periods that determine the maximum 1 or 6 h precipitation rate may also be included in the time periods that determine the maximum 12 h precipitation rate.

The advantages of using the above duration-based method are that (1) it avoids the use of *ad hoc* thresholds that are independent of the energy system for defining drought events; (2) it can be used to calculate droughts for any length of duration desired; since drought intensity generally decreases with duration, droughts can then be characterized out to time periods long enough that they will no longer impact the energy system; (3) whereas threshold-dependent intensity-based methods or discrete duration-based methods can produce droughts that differ considerably depending on the thresholds used, or that differ from what one would intuitively consider the duration to be (e.g., an extended period of drought interrupted by a single time step of above average production that breaks the drought into two shorter segments; or a time period with continuous negative power anomalies that is longer than the fixed duration used), the proposed method avoids these issues entirely by avoiding the use of thresholds and by calculating droughts independently for all durations out to a maximum value beyond which the drought intensities are sufficiently small to no longer be important.

III. ANALYSIS DOMAINS

The domains and sub-regions of this study are shown in Fig. 1. The largest sub-regions, shown in Fig. 1(a), are close approximations of the major U.S and Canadian Eastern and Western Interconnects (EIC and WIC, respectively), the Energy Reliability Council of Texas (ERCOT) Interconnect, and the Quebec Interconnection (QIC). These electric grid interconnects are regions over which all electric utilities are electrically tied together during normal system conditions, operating at a synchronized frequency, such that electric power can potentially be shared given sufficient transmission. Analyses will also be presented using smaller sub-domains within the EIC and WIC shown in Fig. 1(b). Although comprised of combinations of individual states, these regions approximately match existing Regional Transmission Operators (RTOs), Independent System Operators (ISOs), and

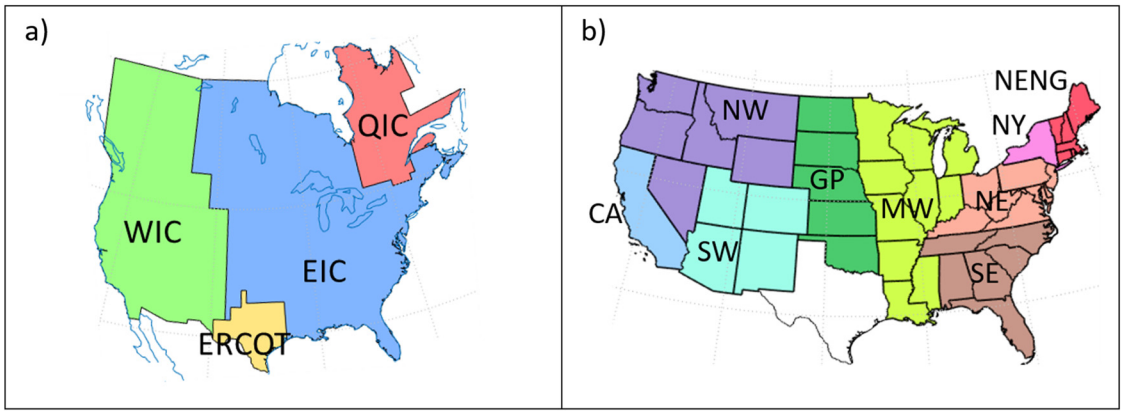

FIG. 1. (a) Interconnect regions used in the drought analysis, including the four major electric grid interconnects (Western Interconnect WIC, green; Eastern Interconnect EIC blue; Texas Interconnect ERCOT, yellow; and Quebec Interconnect QIC, red); (b) Sub-regions used for drought spatial analyses. From east to west the regions are: New England (NENG), New York (NY), Northeast (NE), Southeast (SE), Midwest (MW), Great Plains (GP), Southwest (SW), Northwest (NW), and California (CA). The ERCOT domain is used in place of Texas.

regional power pools, over which electricity can be traded within transmission constraints (https://www.ferc.gov/electric-power-markets) to help balance demand and supply and keep the grid stable. Solar droughts were analyzed using only the overland ERA5 grid points in the areas shown in Fig. 1. However, to roughly include the potential contributions of offshore wind energy, the three nearest over-water ERA5 grid points (extending ∼75 km offshore) along the U.S. and Canadian coast lines including the Great Lakes were included when evaluating wind energy droughts.

IV. DATASETS

This study is based on a bias-corrected version of the ERA5 reanalysis. The ERA5 reanalysis,[34] based on the ECMWF IFS model, has a native horizontal resolution of ∼31 km, and is provided on a uniform 0.25° grid, with hourly time resolution. The analysis by Wilczak *et al.*[1] quantified the accuracy of the ERA5 for drought analysis purpose and then developed corrections to the ERA5 reanalysis so that it more accurately portrays drought events. That analysis used SURFRAD, SOLRAD, and DOE ARM-SGP observations to determine that ERA5-derived values of daily averaged solar power (24 h averages) using fixed-tilt solar panels were biased high in all seasons except JJA, with a maximum mean bias of approximately 25% in DJF. That analysis also determined that during solar energy drought events the uncorrected ERA5-derived solar power was biased high by up to 40% for a range of durations. Those biases were found to be spatially consistent across the U.S., with only slightly larger values in the southwestern U.S. Monthly quantile-quantile multiplicative binned bias corrections were developed at each observation site in that analysis that eliminated this overestimation, without over-inflating the ERA5-derived solar power variances, and those corrections are now interpolated across the ERA5 grid.[35] Those monthly gridded correction factors are then linearly interpolated to daily values on the entire ERA5 grid. The ERA5 solar CF at each grid point and at each day in the 64-year time series is corrected by multiplying it by the appropriate longitude, latitude, day of year, and CF bin-dependent correction factor.

For wind speed, significant low biases were found for off-shore and all on-shore regions in which hub-height observations were available, except for the northeastern U.S. Unlike the observing system for surface solar irradiance, there is no quasi-uniform observational network for 100 m winds across the contiguous United States (CONUS), with large observational gaps in the southeastern, southwestern, and intermountain western states. Therefore, we choose to apply a simpler spatial variation to the corrections of the ERA5 winds. For locations west of longitude 92 W we correct the ERA5 wind speeds with the mean slope and intercept of six wind networks' aggregate daily wind speed linear regressions, while for longitudes east of 87 W we use the linear regression from eight individual non-coastal NY mesonet sites (see Fig. 14 of Wilczak *et al.*[1]) For intermediate longitudes, we linearly interpolate the slope and intercept between these two sets of values. For offshore winds, we use the average slope and intercept from a set of buoy lidars. These linear bias corrections are then applied to hourly ERA5 100 m wind speeds, and density-adjusted hourly wind power values are calculated using the NREL WindToolkit[36] power curves (using Class I, II and III power curves over land, and an offshore power curve). Finally, the hourly power values are averaged to generate daily bias-corrected power values at each ERA5 grid point in the analysis domain. Without correction, ERA5-derived wind capacity factors in the central and western U.S. and offshore were biased low by 20%, and these biases were removed through the linear regression correction. To reduce the potential for over-inflation of the ERA5 variances, regressions were derived from network spatial aggregates of daily averaged wind speeds, and wind power was then calculated after applying the corrections at hourly resolution.

Limitations of the bias-corrected ERA5-derived solar and wind power dataset (ERA5BC) include its coarse spatial resolution, and that it does not account for snow on solar panels, nor icing of wind turbine blades. In addition, no explicit attempt is made to incorporate turbine wake effects, which would depend on the unknown design characteristics of future wind plants.

V. ANNUAL CF MAPS, TRENDS, WIND, AND SOLAR CORRELATION

Annual average bias-corrected solar and wind capacity factors (CF) from ERA5BC are shown in Fig. 2. Solar CFs are largest in the

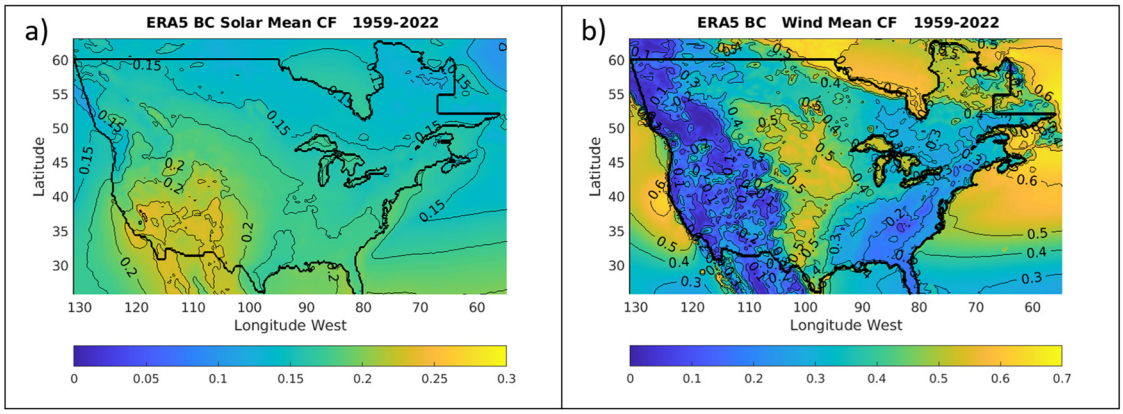

FIG. 2. Mean ERA5-derived bias corrected (ERA5BC) capacity factors for (a) solar and (b) wind. Contour intervals are 0.025 for solar and 0.1 for wind.

southwestern U.S., while wind CFs are greatest offshore and in the Great Plains region of the central U.S. and Canada.

Time series of annual solar and wind CFs, averaged over the entire 4-Interconnect domain, show modest trends over the 64-year period between 1959 and 2022 (Fig. 3), with the wind CF decreasing by 2.3% while solar decreases by 1.7%. The two time series vary smoothly with time, with no obvious step-like jumps that could be attributed to new satellite observing systems becoming available for assimilation. The spatial variations of the ERA5BC CF trends are shown in Fig. 4, where a larger spatial variability is found for the wind CF trends relative to those for solar. Decreases of wind CF tend to be larger for the eastern U.S. Decreases of the solar CF are also larger for the eastern U.S. and near zero for the western portion of the domain up to latitudes reaching 50° N.

As will be shown later, the trends in CFs, although not insignificant, are nevertheless small enough that they will not materially affect the calculation of wind and solar energy drought intensities for short

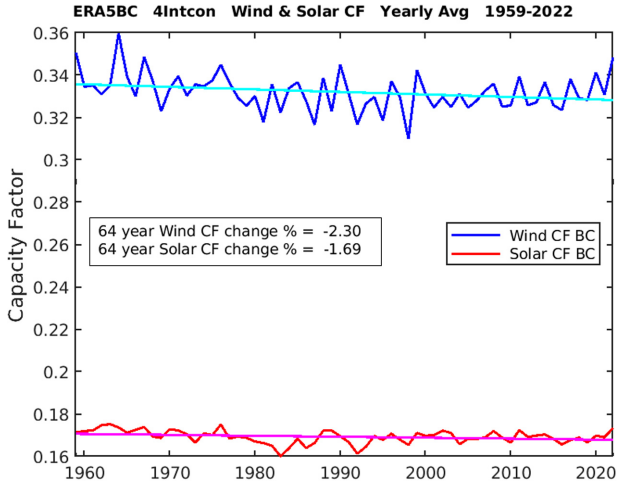

FIG. 3. Wind (blue) and Solar (red) annual CFs averaged over the 4-interconnect domain. Least squares regressions give a 2.30% decrease for the wind CF between 1959 and 2022 (cyan), and 1.69% for the solar CF (magenta).

to moderate duration severe droughts. However, longer duration (~90 days) drought intensities become small enough that the trends may affect the detection of the worst-case droughts, producing a slight preferential selection of later years in the time-series. This however is a real effect present in the reanalysis-derived wind and solar CF ERA5 and ERA5BC data (bias correction has little effect on the trends).

In the analysis that follows, solar and wind droughts are examined using a variety of analysis tools, including annual cycles for various regions, maps of worst-case droughts for selected regions and for several selected durations, IDF curves for each of the regions, correlation maps and scatter plots of wind and solar generation, and scatter plots to examine the interdependence of wind and solar generation with temperature. In addition to analyzing droughts over the entire annual cycle, we also focus on the winter (DJF) and summer (JJA) seasons, which are of interest because solar generation is minimum in winter while wind generation is smallest in summer. Also, electric loads typically have two seasonal maxima, one in winter (for heating) and one in summer (for air conditioning) during which it would be more challenging to balance electric grids with large wind or solar generation.

VI. ANNUAL CYCLE DIAGNOSTICS, SCATTER PLOTS, CORRELATION MAPS, AND HISTOGRAMS

As examples of small and large potential grid balancing areas, results are shown for the State of New York (NY, which is also its own ISO), and for the CONUS. The annual cycles (solid lines) of wind (blue) and solar (red) normalized power are shown in Fig. 5, using 4-harmonic fits to the 64-year average normalized power for each day-of-year (DOY), as described in Wilczak *et al.*[1] In addition, the standard deviation is denoted by the darker shaded area, with the minimum and maximum daily normalized power (henceforth power) values for each DOY by the lighter shaded area.

For NY, the annual cycles of solar and wind power have several notable features. The solar power standard deviation is relatively small during winter, when the mean power is small. It is also small during summer when the mean power is near its maximum. The solar power standard deviation for NY is larger during autumn and is greatest in the spring. The smallest DOY minimum solar power values occur in winter, while those in summer are 3–5 times larger. In contrast, for wind the standard deviations are only smaller in summer, while

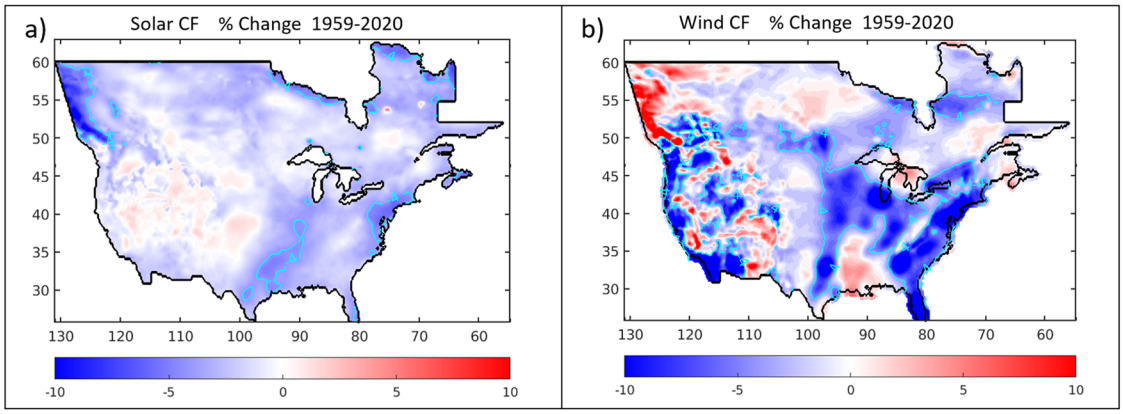

FIG. 4. Maps of (a) percent wind CF change and (b) percent solar CF change over the 1959–2022 period. Cyan contours denote a change of −4%.

minimum values near zero can occur in any season. Wind power is seen to be more variable than solar, with larger standard deviations and more extreme maxima. Minimum DOY power values for wind and for solar can drop to only a few percent of the annual averaged mean generation.

For CONUS, the larger region produces different annual variability characteristics. Its solar power standard deviations are nearly constant through most of the annual cycle, smaller only in summer, while the smallest DOY minima again occur in winter. For wind, the standard deviations are also smaller only in summer, while the smallest DOY minima are nearly equal in all seasons. The smaller standard deviations and more compressed range of minimum and maximum values for the CONUS region, for both wind and solar, highlights the advantages of having a larger area to balance the grid. As for NY, wind has greater variability than solar, with a larger standard deviation for every DOY and a larger spread of minimum and maximum values.

Also shown are the annual cycles of a mix of wind and solar generation, where both contribute equal amounts to the total long-term energy generation [Figs. 5(e) and 5(f)]. There are several benefits to this mix (identified as W50%+S50%). In both regions, the annual cycles have flatter annual variation of mean generation than either wind or solar alone. Both regions' standard deviations are smaller than wind and close to those of solar. Both regions' smallest DOY minimum values (occurring in winter) are greater than wind or solar alone. Although it has flatter profiles, the mix of wind and solar for both regions has approximately 20% above average generation in the spring, when energy demand is typically low, and approximately 10% below average generation in late summer and early winter, when energy demand is often high.

In addition to the characteristics of wind and solar droughts treated independently, the characteristics of their co-variability also will be important for any electric grid system that has generation from both sources. One simple way to assess this co-variability is through maps of the temporal correlation coefficient of wind and solar normalized power. This is shown in Fig. 6 for the entire analysis domain for the daily-averaged data [Fig. 6(a)], and after applying running means of 10 and 30 days [Figs. 6(b) and 6(c)]. Ideally, wind and solar generation would be negatively correlated. Although overall wind and solar are negatively correlated, it is apparent that there are strong spatial patterns to the correlations, with both positive and negative values that depend on location and running mean duration. Specifically, the correlation is mostly positive in the southwest U.S., which is largely a result of the wind and solar mean generation increasing in tandem from January until April, and then both decreasing from April through July (not shown). Also, the magnitudes of the correlations (of either sign) at each grid point tend to increase with increasing durations, as noise associated with weather events decreases relative to the seasonal cycles. For the 30-day running mean, the range of negative and positive values, and the preponderance of negative values near −0.5, are similar to those found by Wohland *et al.*[37] for Europe and North Africa on a seasonal timescale using different reanalysis datasets.

Another useful way to examine the co-dependence of wind and solar generation is through simple scatter plots. Figure 7 shows scatter plots of wind and solar percent of average power generation, again for the NY and CONUS regions, for daily values and using 30-day running mean averages. In each plot, the average generation value of 100% is denoted by the solid horizontal and vertical black lines, and any power value in a W50%+S50% system that is less than average will lie below the dashed line. Ideally wind and solar would have a large negative correlation, and no values close to the bottom left corner of each plot, where wind and solar simultaneously reach zero generation. For the NY region and a duration period of 1 day [Fig. 7(a)], the correlation is negative but moderately small (Corr = −0.323), and there are numerous days with wind and solar generation simultaneously less than 25% of their annual average generation. For the 30-day running mean [Fig. 7(c)], the negative correlation is more substantial (Corr = −0.645). The worst droughts of 30 days duration have much larger normalized power values for both wind and solar, with no points where wind and solar are simultaneously less than 75% of average generation. For the CONUS region and a duration period of 1 day [Fig. 7(b)], the correlation is similar to that for NY, but the worst simultaneous wind and solar drought days are less severe, with no points where wind and solar are simultaneously less than approximately 50% of average generation. For the 30-day running mean [Fig. 7(d)], the negative correlation (Corr=-0.513) is smaller than for NY, but the most extreme 30-day duration droughts are slightly improved, with no points where wind and solar are simultaneously less than approximately 80% of average generation. We note that for

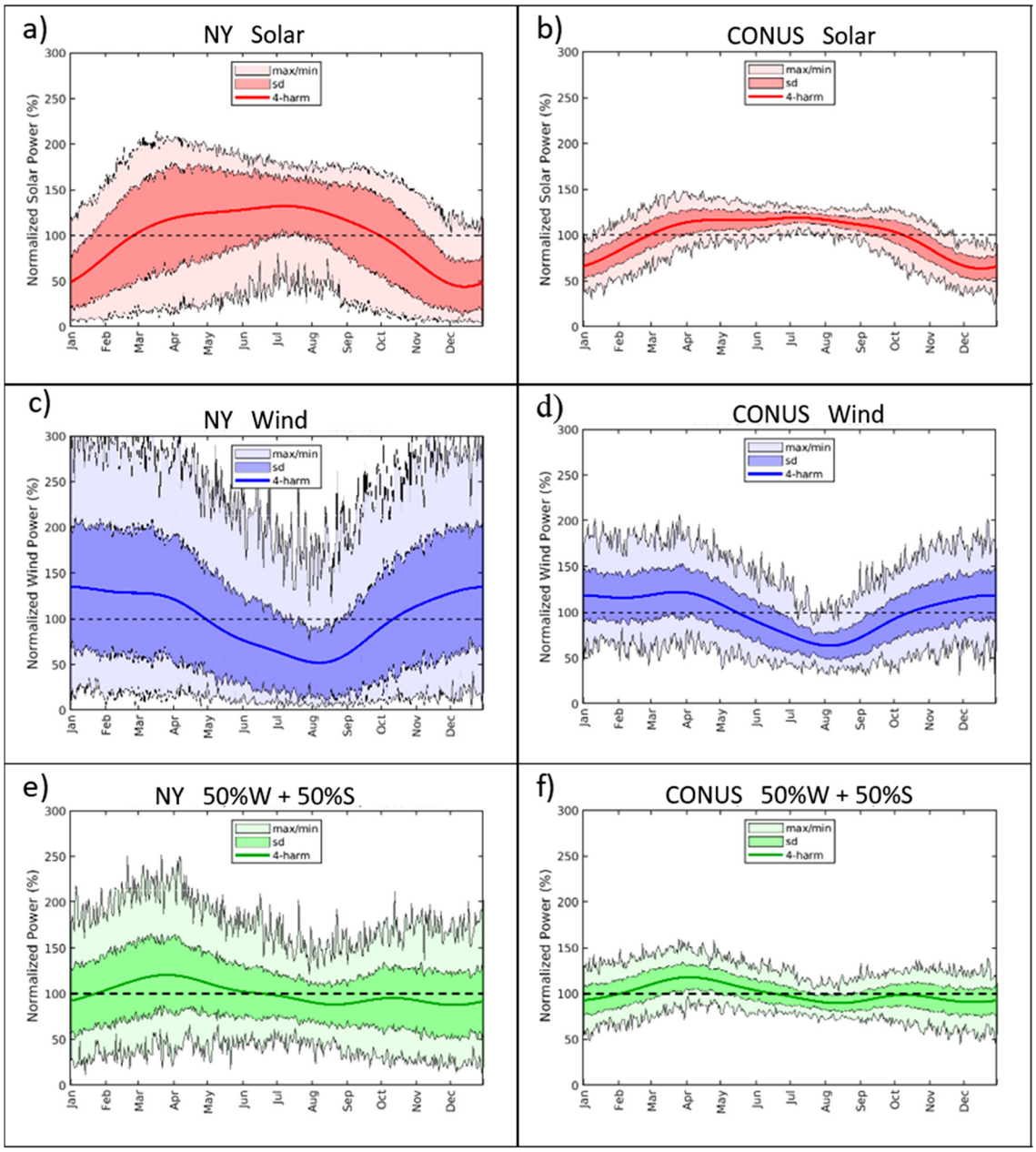

FIG. 5. Annual cycles of daily normalized power including four-harmonic fits (dark colored lines), standard deviations (medium shaded areas), and the DOY maximum and minimum values (light shaded areas). Dashed horizontal lines correspond to the long-term mean power, for (a) NY region solar, (b) CONUS solar, (c) NY wind, (d) CONUS wind, (e) NY mix of 50% wind and 50% solar, and (f) CONUS mix of 50% wind and 50% solar.

longer durations and larger regions [e.g., Fig. 7(d)] that limits to the maximum positive values of both wind (∼150%) and solar (∼125%) are present, presumably due to the physical limitations on the maximum power that either can produce in perfect conditions.

Histograms of ERA5BC daily power values (Fig. 8) demonstrate that wind and solar can have highly non-Gaussian distributions, as suggested by the previous scatter plots. Despite this, when including data from all seasons, differences between the means and medians are always less than 15% in each of the geographic regions we analyze. Histograms using data subset by season are always much closer to Gaussian, with differences between the mean and median of only a few percent. For the W50%+S50% scenario, distributions from the complete dataset, as well when subset by season, are also always close to Gaussian, with differences between the mean and median again of

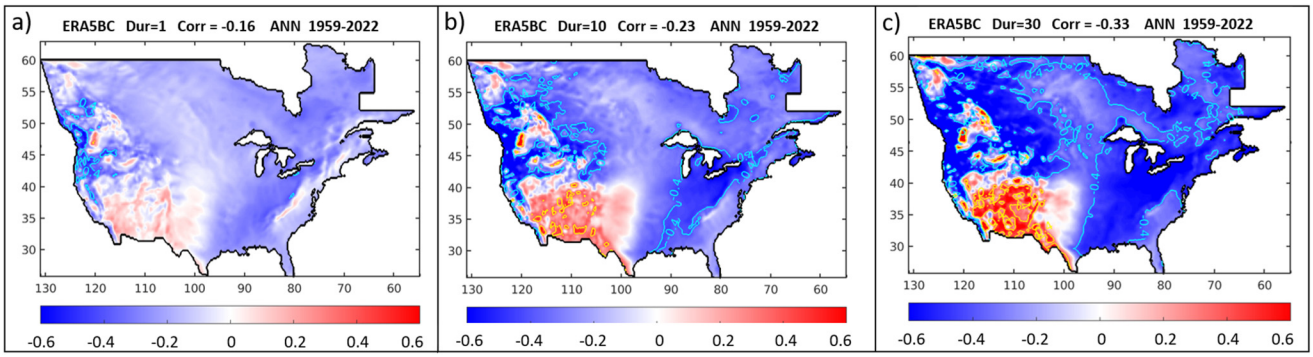

FIG. 6. Correlation coefficients of wind and solar power, for running mean durations of (a) 1, (b) 10, and (c) 30 days. Correlation coefficient values of ±0.4 are contoured.

only a few percent. Because the difference between the mean and the median are small, either can be used to determine what the percent of the "normal" generation would be. This is different from precipitation, which can have much larger differences between mean and median, and can lead to ambiguities in interpreting the percent of normal precipitation.[38] In addition, the widely varying shapes to the distributions indicates that if one were to take an extreme value approach for estimating return periods, that it would be inappropriate to assume a single extreme value distribution type to fit each of those histogram shapes.

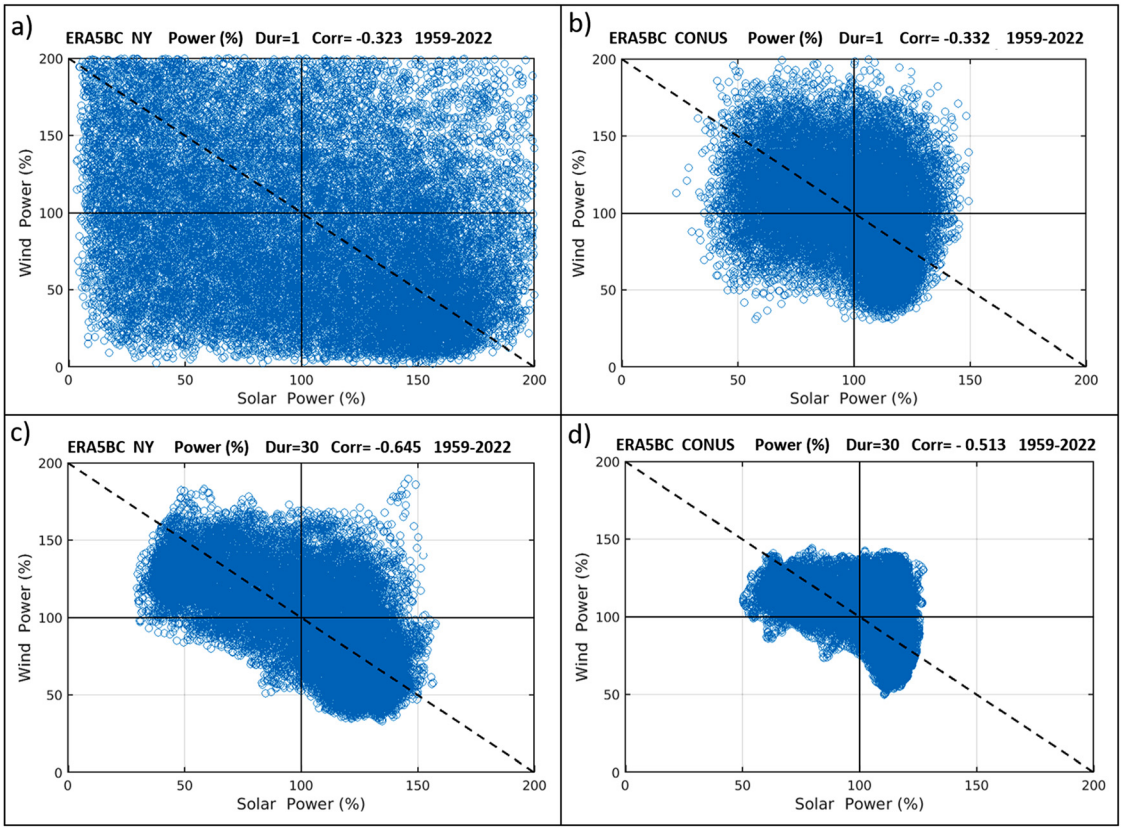

FIG. 7. Scatter plots of normalized wind and solar power, where 100% is the mean value over the 64-year analysis period, for the (a) NY region with duration = 1 day, (b) CONUS with duration = 1 day, (c) NY with duration = 30 days, (d) CONUS with duration = 30 days. Any power value in a W50%+S50% system that is less than the long-term mean will lie below the black dashed line. For ease of comparison, all four panels have the same axes limits, which results in some large positive normalized power values being off-scale in panel (a).

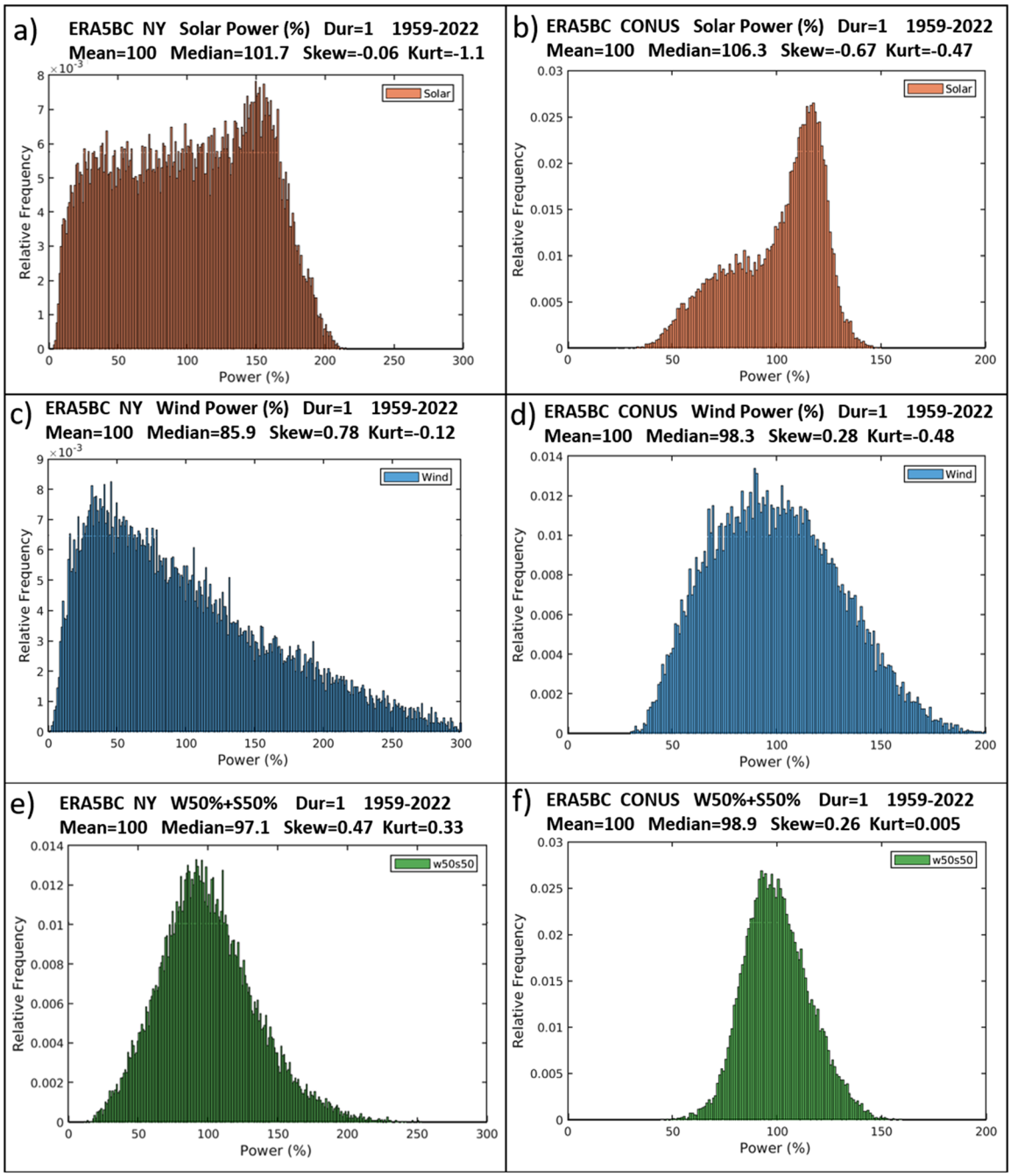

FIG. 8. Histograms of daily values of normalized power, for the (a) NY region solar, (b) CONUS solar, (c) NY wind, (d) CONUS wind, (e) NY mix of 50% wind and 50% solar, and (f) CONUS mix of 50% wind and 50% solar.

VII. DROUGHT MAPS, OVERBUILD FACTORS, AND STORAGE DISCHARGE LIMITS

We analyze droughts both as averages over regions that represent real or hypothetical grid balancing areas, as well as on a grid point basis that then can be shown as maps. For the regional averages, our drought definition uses area-mean normalized power generation, which would be the percent of the long-term mean power generated seen by the transmission operator for that regional balancing area. To display maps of power generation during drought events there are two options. The first is to show the percent of average power generation

calculated at each grid point, which then quantifies the drought amplitude on a *local* basis. However, for regions over which the long-term mean generation has significant geographic variation, the percent of power generated at each grid point will not accurately depict how much power each grid point contributes to the regional mean generation. When creating maps to assess drought impacts on a regional balancing area, it can be more informative to simply show the CFs at each grid point, which then indicates the contribution of each grid point to the *regional* average generation. For these reasons, in some parts of the analysis we show maps of both normalized power and of CFs.

The spatial characteristics of wind and solar energy droughts are investigated through drought maps of the most extreme events. A map of normalized solar power (where a value of 100% equals the long-term mean production) for the most extreme one-day duration drought day (20 Nov 1988) for the NY region [Fig. 9(a)] shows the spatial reach of the drought area affecting NY. The 25% contour line (cyan) encompasses parts of Canada, extends south to the Gulf Coast, and west into the central U.S., while the NY average solar power generation on that day is 3.5% of its long-term mean. Maps of the corresponding actual daily averaged CF on this same day (not shown) have a NY region average of 0.006, while large solar CFs reaching 0.25 are present in the south-central and southwestern US. For comparison, the corresponding plot for the most extreme solar drought day for the larger hypothetical CONUS balancing area is shown in Fig. 9(b). On this day (28 Dec 1992), most of the CONUS domain has solar power values less than 25% of average, including much of the high solar resource area in the southwest U. S., with the CONUS mean solar generation being 23.6%, and the corresponding mean CF = 0.044.

For wind power, the most extreme drought day (04 Aug 1996) for the NY region [Fig. 9(c)] shows the drought area extending through a large portion of the eastern U. S. and Canada. The NY average wind power generation is only 1.7% of its long-term mean. Maps of the corresponding daily CF on this same day (not shown) indicate a mean NY CF of 0.005, while very large wind CFs greater than 0.6 are present in the high wind resource in the central U.S. and Canada. In comparison, the most extreme wind drought day for the CONUS (07 Sep 1993) has a mean generation of 30.6% [Fig. 9(d)], with a few areas within the CONUS in the western states having above average generation. The corresponding CONUS mean CF for this day is 0.094. These maps illustrate that (1) for small regions the most extreme one-day droughts can have very small amounts of wind and solar generation; (2) on those drought days, small regions could take advantage of above average generation in surrounding regions if transmission were available. However, if transmission did link these regions together, the new

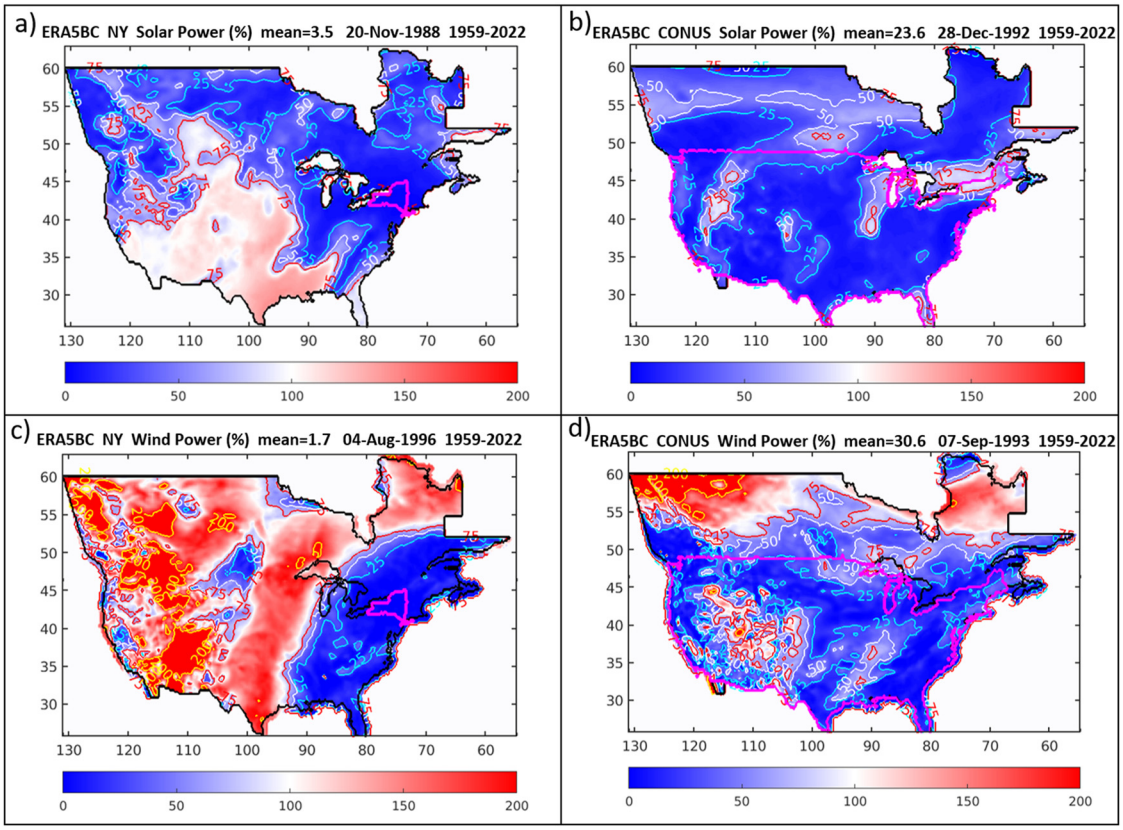

FIG. 9. Maps of normalized power on the days with the smallest values (most extreme solar and wind droughts) in the 64-year data record, for the (a) NY region solar, (b) CONUS solar, (c) NY wind, (d) CONUS wind, where the regions are outlined in magenta. Normalized power is displayed which quantifies the drought amplitude locally at each ERA5BC grid point. Contours are drawn for values of 25% (cyan), 50% (white), 75% (red), and 200% (yellow) of the long-term mean generation. Titles provide the mean normalized power for the region on the worst drought day and the date of its occurrence.

worst drought days for that larger region are still substantial, although much better than for the small regions alone (e.g., from Fig. 9 for the CONUS compared to NY, 23.6% vs 3.5% for solar, and 30.6% vs 1.7% for wind).

The variability of renewable power generation can be dealt with through transmission, storage, or over-building of capacity. Although the present study focuses on wind and solar generation droughts and does not explicitly consider the full energy system or storage, nevertheless, one can infer from the characteristics of droughts some of their general impacts on energy system and storage requirements. We consider two limiting cases, the first with no storage, where drought events are mitigated through over-building of capacity; and second, where no over-building of capacity occurs, and drought events are mitigated through discharge of presumed storage. These two cases are applied to a hypothetical energy system for a region dependent only on solar power, only on wind power, or for the (W50%+S50%) combination of both, with no other types of generation, and with no transmission to import electricity from outside the region, but sufficient transmission within the region. In our definition, an over-build factor equal to one occurs when the daily mean generation is equal to the long-term mean generation, signifying that no over-building is needed.

For the case of no storage, the minimum amount of over-building required to bring the level of generation up to the long-term mean generation will be determined by the drought with the smallest amount of energy produced, which occurs for the shortest 1-day duration, and is therefore equal to the inverse of the minimum daily normalized power generation. Over-building multiplicative factors for solar, wind, and for the W50%+S50% scenario, are shown in Fig. 10(a) for each of the regions. For NY, for which the smallest daily solar normalized generation was shown to be 3.5% of the long-term mean generation in Fig. 9, one would have to install $1/0.035 = 28.6$ times more solar capacity than that needed on an average day to produce the same amount of energy. In some regions, the over-build factor is larger for wind than solar, in others the reverse. In all regions, the over-build factor for the W50%+S50% scenario is much reduced. Also, the over-build factor decreases substantially as the size of the region increases, approaching a factor of two for the largest regions, with a value of 2.2 for the CONUS.

For the second limiting case, in which periods of generation less than the long-term mean generation are balanced by discharge of storage, with no over-building of capacity, the discharge rate required to bring the net power availability back up to the level of the long-term mean generation is simply equal to the difference between 100% and the smallest normalized generation. For the worst NY solar drought day, which has generation equal to 3.5% of its long-term mean, the required storage discharge rate for that day is 96.5% of the long-term mean generation. Values of these maximum discharge rates are shown in Fig. 10(b) for each of the regions. In some regions, the discharge rate is larger for wind only than for solar only, in others the reverse. In all regions, the W50%+S50% scenario has the smallest discharge rate, and the discharge rate decreases as the size of the region increases. If storage were to be provided with hydrogen or other power-to-gas methods, the required conversion rate back to electrical energy would be substantial for this zero over-building case, even for large balancing areas.

These two limiting cases represent theoretical extremes that are unlikely to occur in reality. Realistic low-carbon energy systems will contain some amount of both over-building and multi-day storage, as well as other types of generation including hydropower, nuclear, and geo-thermal, and an optimal mix of those, together with demand response programs, is likely to result in much smaller required levels of over-building and storage discharge capacity than these theoretical limits.

For a large region such as the CONUS, is it possible to mitigate the worst droughts through judicious siting of generation? Figs. 11(a), 11(c), and 11(e) shows the first-, second-, and third-worst one-day solar drought days for the CONUS region, now displaying CFs to show the contribution that each grid point makes to the *regional* average generation. On each of these drought days (first, 28 Dec 1992; second, 27 Dec 1984; third, 29 Dec 1992, one day after the top drought event), in a background of very low CF values, several small areas with moderately higher values stand out. However, there is almost no

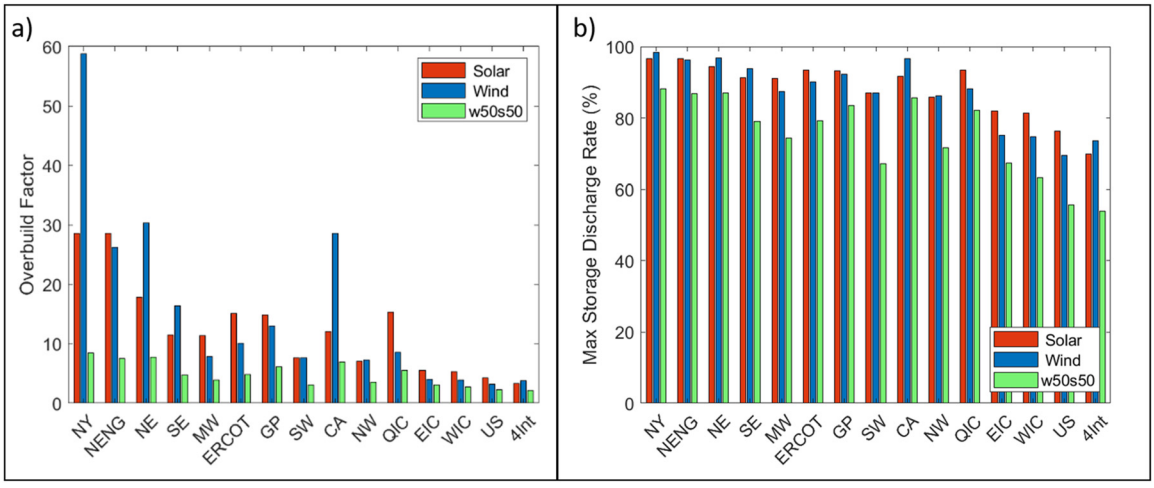

FIG. 10. (a) Over-build factors for the 15 regions analyzed, for solar (red), wind (blue) and the W50%+S50% mix of wind and solar (green) for the case of no storage. (b) Maximum required storage discharge rates for the case of no over-building of capacity as a percent of the long-term mean daily generation.

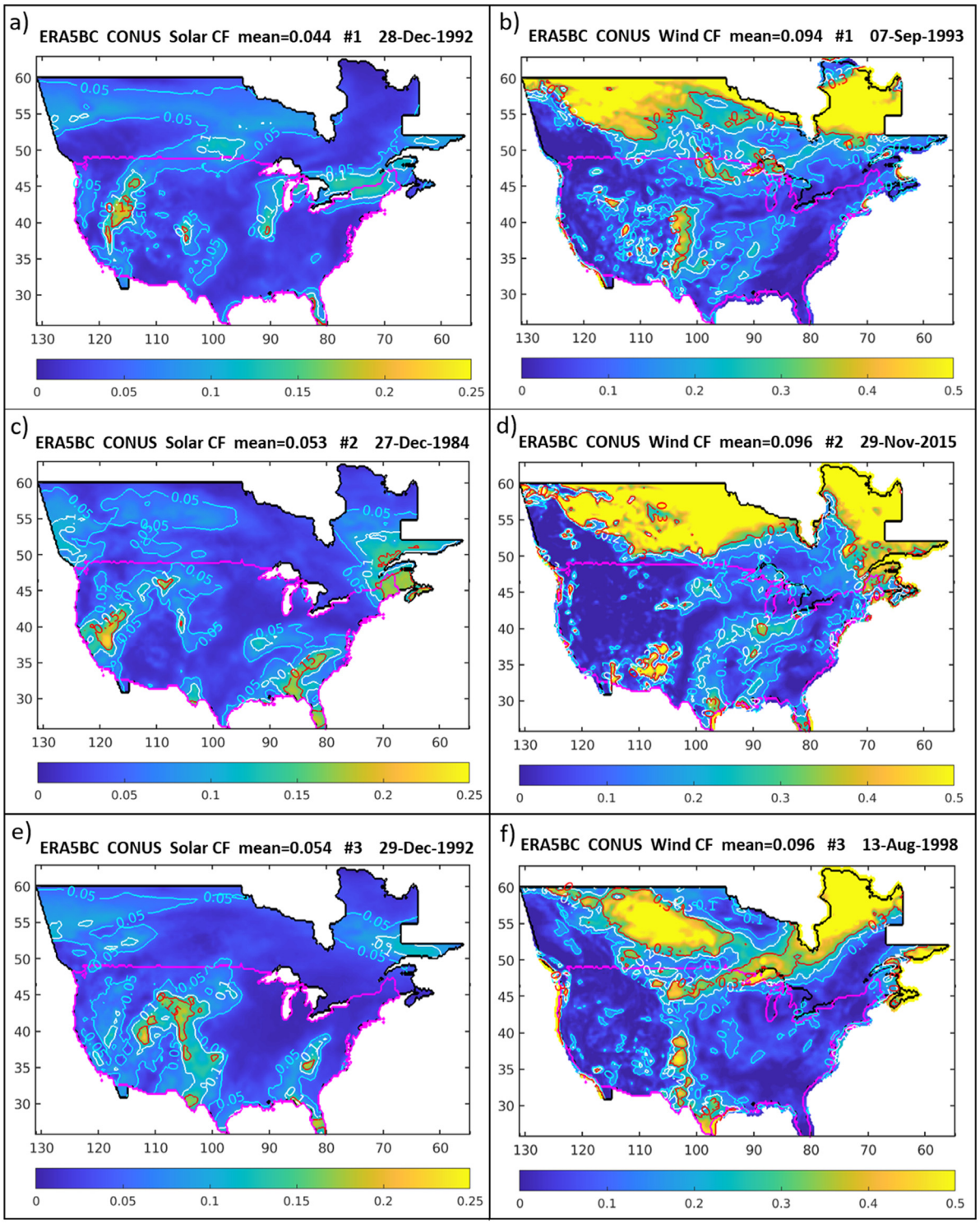

FIG. 11. Maps of daily CF corresponding to the 3 days with the smallest normalized power values (most extreme droughts) for the CONUS region in the 64-year data record, for the (a) solar worst, (b) wind worst, (c) solar second worst, (d) wind second worst, (e) solar third worst, and (f) wind third worst drought days. Contours for solar are drawn for values of 0.05 (cyan), 0.1 (white), and 0.15. Contours for wind are drawn for values of 0.1 (cyan), 0.2 (white), and 0.3. CFs are displayed to show the contribution that each grid point makes to the regional average generation.

overlap of these areas among the top three most intense drought days, and none of the days have large CFs in the southwest U.S. high resource area. Optimizing the location of solar generators for short-duration droughts is difficult, due to the chaotic nature of short-term weather patterns. Instead, spatial diversity of generation would be beneficial for these short-duration solar drought events, as there is no obvious set of optimal locations that span a significant area in which one could overweight generation capacity to mitigate them. For wind [Figs. 11(b), 11(d), and 11(f)], the results are more ambiguous, as there is some tendency for higher CFs in the central U.S.

To gain additional insights into siting optimization for short-term droughts, we show in Fig. 12 CF maps of the average of the 10 worst solar and wind droughts that occurred within the CONUS region. For solar [Fig. 12(a)], although there are some small areas with higher CFs, such as in the lee of the southern Sierra Madre mountains east of California and in the lee of the Rocky Mountains, and in Florida, overall the distribution of CFs is fairly flat. Noticeably, relatively high CFs are not present throughout most of the southwest U.S., despite it being a high solar resource region. In comparison, the wind CFs [Fig. 12(b)] have a more pronounced region of high CFs in the Great Plains and Texas, coincident with the higher mean wind resource in those regions. This suggests that in order to mitigate CONUS short-term droughts there may be value in over-weighting wind generation in the high wind resource central U.S, while the same is not true for over-weighting solar capacity in the high resource SW region.

To expand the analysis of mitigation of wind and solar droughts to include longer durations, we consider the single most intense droughts of durations 1, 10, and 30 days for the high resource southwest U. S. region for solar, and a combination of the Texas and Great Plains (TXGP) regions for wind that were defined previously in Fig. 1.

Wind capacity factor maps for all four seasons combined for TXGP [Fig. 13(b)] show that the most intense 1-day duration drought has a regionally averaged CF of 0.104 (i.e., averaged over the area outlined in magenta), slightly higher than the CONUS-mean CF for the most intense CONUS wind drought, which has CF = 0.094 as discussed for Fig. 9. In other words, surprisingly the worst 1-day wind drought averaged over the smaller TXGP region is somewhat better than the worst 1-day drought over the larger CONUS region. For 10- and 30-day droughts this unexpected behavior is even more pronounced, with the most intense TXGP droughts having CF values of 0.215 and 0.273 [Figs. 13(d) and 13(f)], while the corresponding worst 10- and 30-day CONUS drought CFs are only 0.133 and 0.155. In addition, it can be seen that the CF values at grid points within the TXGP region are larger than the CF values across most of the rest of the CONUS domain, even though the 10- and 30-day drought periods were selected based on the TXGP region having its lowest generation over the 64-year analysis period.

A similar analysis but for solar in the high resource southwest U. S. shows that, like wind in the TXGP region, its CFs during its worst droughts are larger than the CONUS as a whole, but now only for the longer 10-day and 30-day drought durations. Specifically, the most intense 1-day duration drought has a mean CF of 0.029 [Fig. 13(a)], which is worse than the value of 0.044 found for the most intense CONUS solar drought discussed for Fig. 9. In contrast, the most intense SW 10-day and 30-day duration droughts have mean CF values of 0.099 and 0.128 [Figs. 13(c) and 13(e)], which are larger than their corresponding worst 10- and 30-day CONUS drought CFs of 0.082 and 0.094.

To summarize, to mitigate the most intense wind droughts of all durations across the CONUS, it would be beneficial to overweight wind capacity in the Texas and Great Plains regions. This is because the wind resource is so extraordinarily plentiful in those regions that even during their worst droughts of any duration, their wind production would nevertheless be better than the CONUS average production. For the mitigation of very short-duration solar droughts, spatially distributed generation would be advantageous. However, there is a crossover point between 1 and 10-days duration, beyond which an over-weighting of generation in the SW high mean resource region would be advantageous for CONUS solar drought mitigation.

VIII. INTENSITY–DURATION–FREQUENCY (IDF) CURVES

IDF curves are generated for both drought and "flood" events using the method described in Sec. II. Here, the term flood is used in the sense of a state of abundant flow or volume, which can have either positive or negative connotations. We choose to show both droughts and floods in the IDF diagrams, because flood events can present

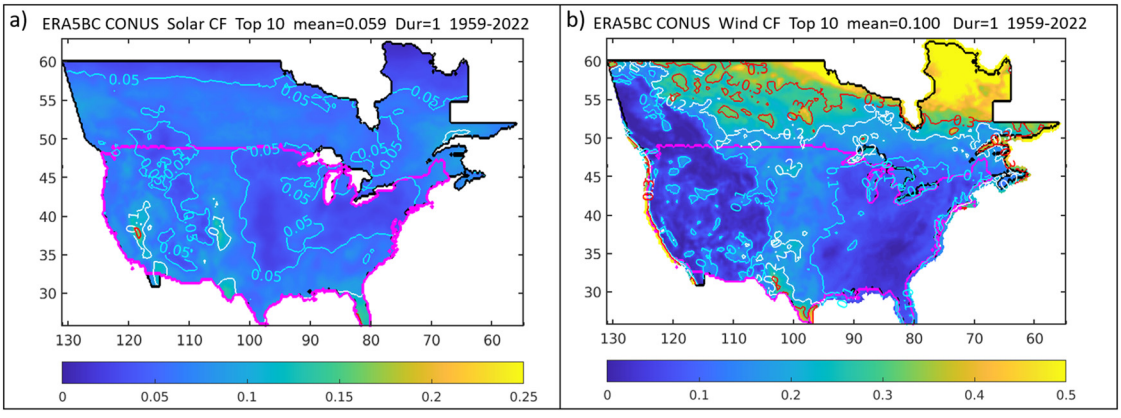

FIG. 12. As in Fig. 11 except for the average of the 10 most intense 1-day droughts for (a) solar, and (b) wind.

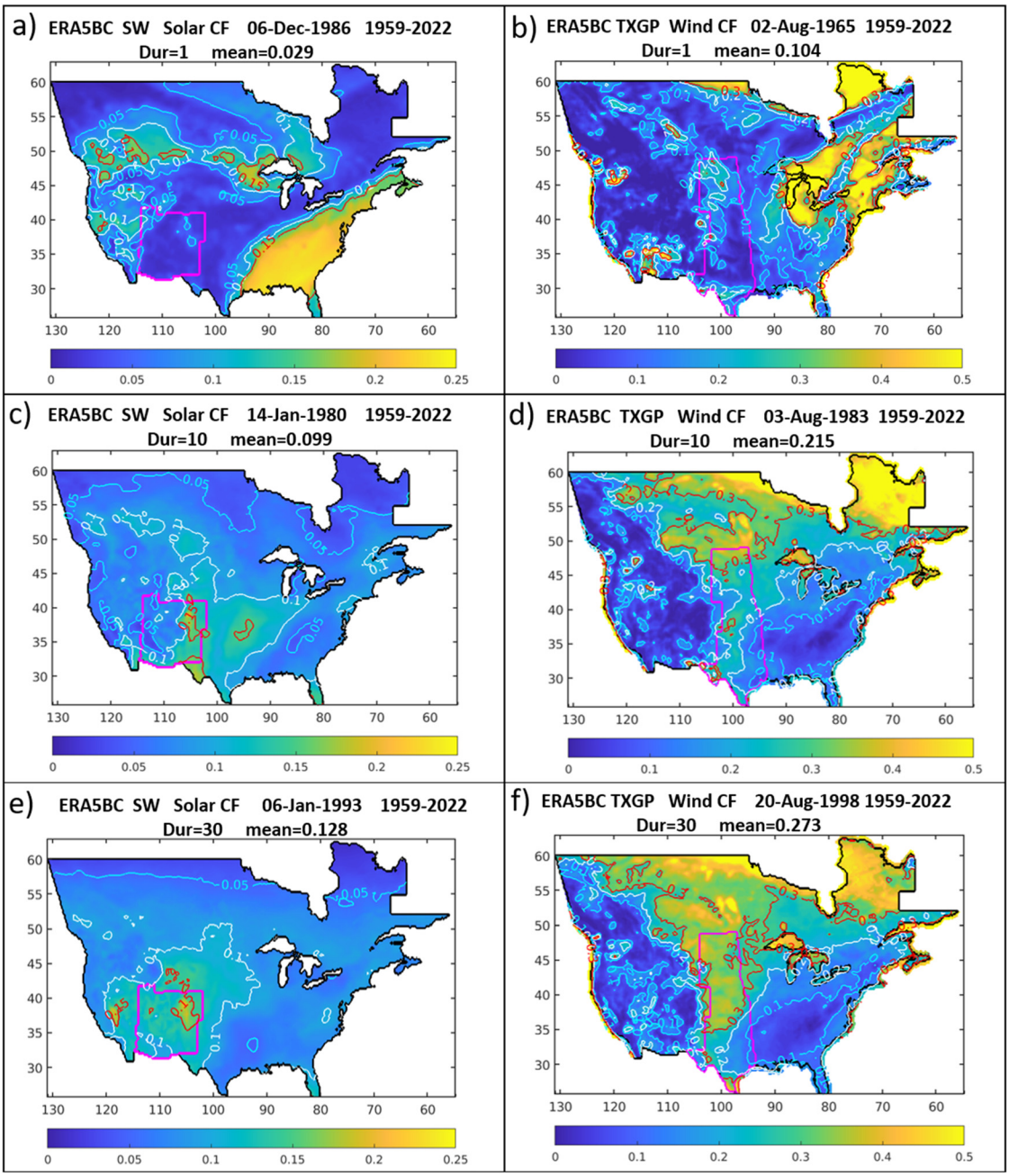

FIG. 13. Maps of CF corresponding to the smallest normalized power values (most extreme droughts) in the 64-year analysis period, for solar droughts in the SW region with durations of (a) 1 day, (c) 10 days, and (e) 30 days, and for wind droughts in the combined TXGP region with durations of (b) 1 day, (d) 10 days, and (f) 30 days. Contours for solar are drawn for values of 0.05 (cyan), 0.1 (white), and 0.15 (red). Contours for wind are drawn for values of 0.1 (cyan), 0.2 (white), and 0.3. The SW and TXGP regions are outlined in magenta.

opportunities to recharge storage, because they may create transmission congestion problems that present challenges for electric grid design and operation, or because they may result in curtailment of generation if no methods are found to make use of the excess generation.

A. Return periods

IDF curves for return periods of T = 4, 16, and 65 years are shown in Fig. 14 for the NY and CONUS regions. For both regions, and for solar, wind, or the W50%+S50% scenario, the T65 year curve (solid lines) normalized power drought values are shifted lower by approximately 5%–15%

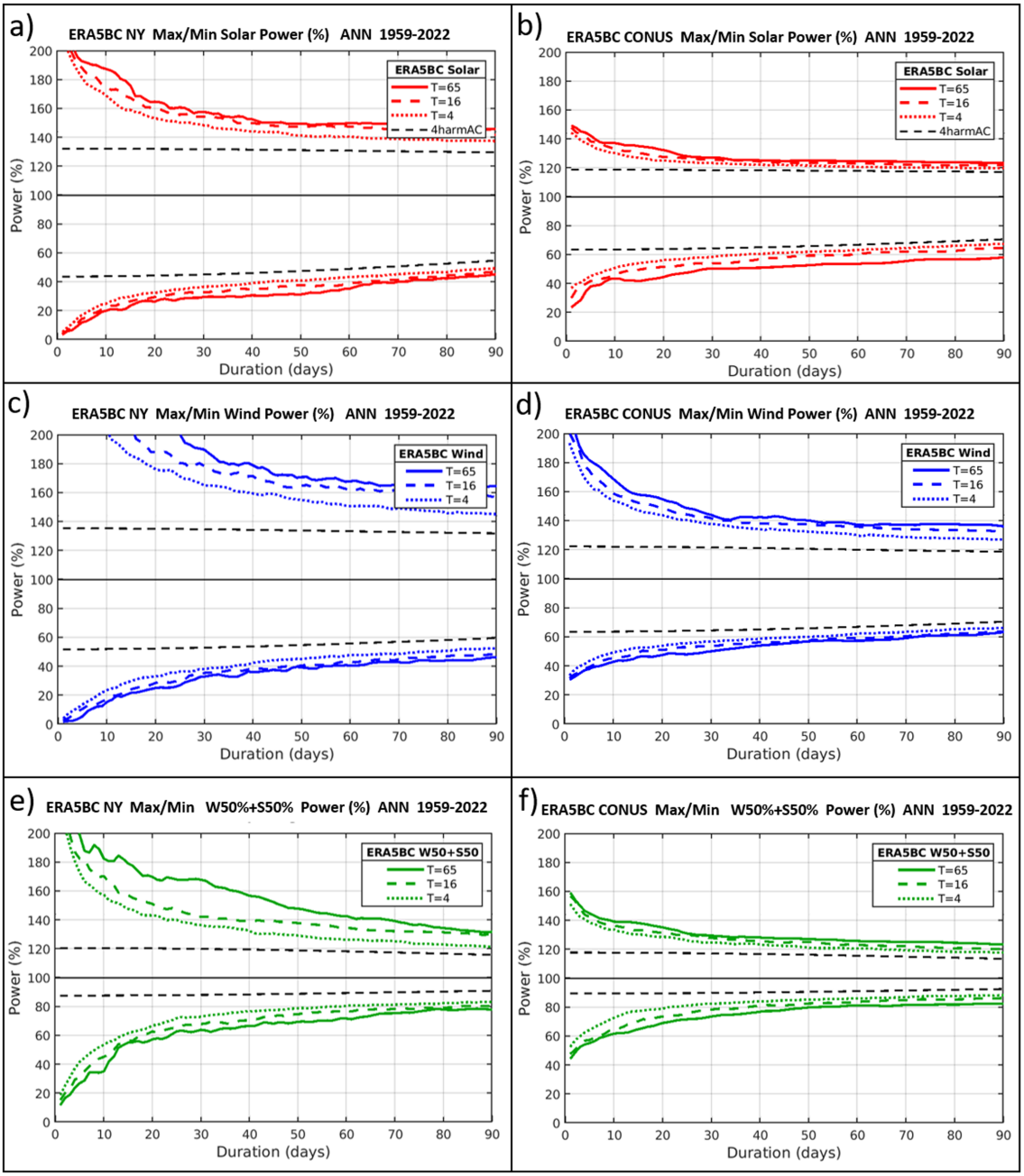

FIG. 14. Intensity–duration–frequency diagrams of the largest and smallest normalized power values in the 64-year analysis period for the (a) NY region solar, (b) CONUS solar, (c) NY wind, (d) CONUS wind, (e) NY mix of 50% wind and 50% solar, and (f) CONUS mix of 50% wind and 50% solar. The red, blue, and green solid curves have a return period of 65 years, the dashed curves 16 years, and the dotted curves 4 years. The black dashed curves in each panel are the contributions of the mean seasonal cycles to the drought and flood events.

of normalized power relative to the T4 year values. Of interest is that these differences are very similar for both the small NY and large CONUS region. Because the W50%+S50% drought intensities are smaller than either wind or solar alone, a constant offset of the T65 curve from the T4 curve translates to a larger relative percentage spread between them.

We note that for the CONUS region W50%+S50% scenario, at a duration of 10–15 days [Fig. 14(f)], the T65 power generation is approximately 60% while for T4 it is near 75%. Using the T4 value will overestimate the amount of power available by 25% [(75–60)/60] if we take the T65 value as the more accurate value. If one considers the

shortfall of energy from the perspective of the amount of energy from storage that would need to be supplied to cover the deficit, these shortfalls are 100% minus the generation, or 40% and 25% for the T65 and T4 return periods. The underestimate in the amount of storage needed is now 37.5% [(40–25)/40] again taking the T65 value as the more accurate value. These numbers provide an estimate of the magnitude of the errors that may affect capacity expansion model studies that rely on short meteorological datasets on the order of 4 years in length.

Also shown in Fig. 14 are intensity–duration curves for the worst droughts and floods, derived from the 4-harmonic fit approximations to the mean seasonal cycles for each of the wind, solar and the W50%+S50% scenarios, shown as the black dashed lines. These curves illustrate the contributions of the mean seasonal cycles to drought events. These contributions decrease slowly as duration increases from 1 to 90 days due to the slowly varying seasonal signal, and eventually reach near zero at 12 months duration. The differences between these curves and the green return period curves represent the impact that short-term weather and interannual climate variability has on enhancing drought events beyond the seasonal cycle component. For flood events, these differences are larger for wind than for solar for both regions, indicating that wind has larger positive variations not associated with the annual cycle than does solar. For drought events, the differences for wind are larger than solar for NY, but similar for the CONUS. For the W50%+S50% scenario drought events, the differences are larger than for either wind alone or solar alone. This results from the fact that for this combination of wind and solar, the amplitude of the mean annual cycle variation (shown in Fig. 5) during the periods of the worst droughts (typically winter) is reduced to a greater degree than are the daily variations.

B. Regional IDF analysis

Next, IDF comparisons are made among different regions, for wind, solar, and the W50%+S50% scenario droughts and floods. For clarity of presentation, only the most extreme (T65) intensity–duration curve is shown. I-D curves for three regions, the CONUS, southeast U.S. (SE), and the Quebec Interconnect (QIC), shown in Fig. 15, demonstrate that drought characteristics can have large regional differences. The curves consist of the lowest and highest percent of the long-term average power produced for each region, as observed within the 64-year ERA5BC dataset, for wind (blue), solar (red) and the mix of 50% wind and 50% solar energy (green). For the CONUS [Fig. 15(a)], solar and wind droughts are found to have nearly equal intensities for most all durations, with the exception that solar droughts are slightly worse than wind for very short 1 to 3-day durations. Wind flood events however have approximately 75% larger intensities than solar. The benefits of the 50%–50% mix of wind and solar is clear, with the amount of power available for these worst observed drought events being nearly 50% greater than wind or solar alone.

For the SE region [Fig. 15(b)], the worst observed wind droughts and floods are more intense than for the CONUS, and wind droughts are considerably more intense than solar droughts for all durations. Also, the separation between the worst wind and solar flood events is greater than for the CONUS. The W50%+S50% scenario again offers considerable benefit over wind or solar generation alone for droughts, but is not as good as solar alone for floods. For the QIC region, the relative intensities of wind and solar droughts and floods are now reversed from those in the SE region, with solar droughts and floods being more intense than wind, in part due to the larger seasonal cycle for solar at more northern latitudes. Of interest is that the W50%+S50% scenario provides little extra benefit compared to wind alone. The QIC region is the only region that shows such marginal benefit from combining wind and solar. I-D curves were examined for the set of 10 worst independent droughts at each duration length, and all showed this same behavior, demonstrating that it is a robust result and not the effect of a single exceptional outlier event. In summary, comparing the I-D curves between the CONUS, SE and QIC regions, it is apparent that wind and solar drought characteristics can have large regional differences.

I-D curves can also be constructed on a seasonal basis, simply by limiting the time windows within which the drought and flood events are found. Characterization of drought events on a seasonal basis may be important for regions where load has a strong seasonal variability. For example, a grid operator in a region with a large summertime peak load associated with air conditioning may especially want to know the characteristics of wind and solar droughts during the warm season. I-D curves for the four separate interconnects (WIC, EIC, QIC, ERCOT) and the combination of these four (4Int) are shown in Fig. 16 for wind and solar, and for the winter (DJF) and summer (JJA) seasons. Because the ERCOT and QIC regions are smaller than the EIC, WIC, or 4Int regions, one would expect them to have more extreme droughts and floods than the larger regions. This is generally the case, although there are multiple exceptions, such as ERCOT solar droughts in winter [Fig. 16(a)] being similar to, or better than, the larger regions

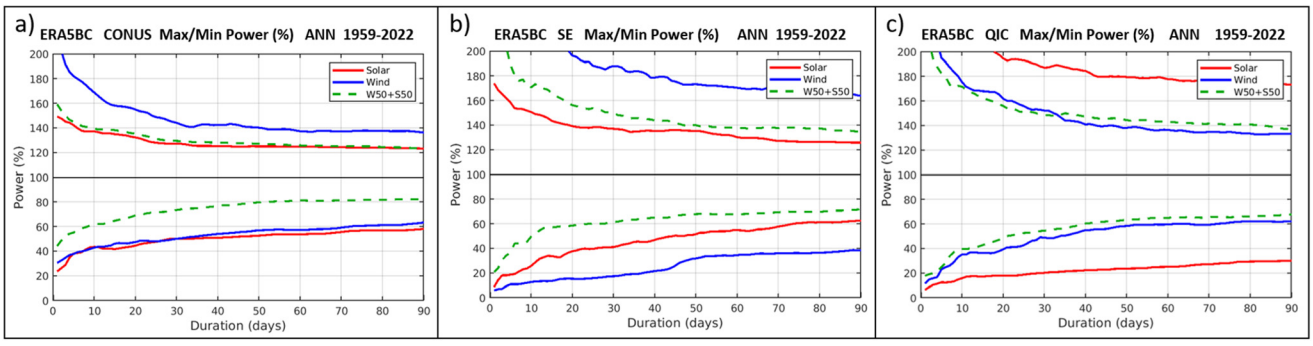

FIG. 15. Intensity–duration diagrams of the largest and smallest normalized power values in the 64-year analysis period, for the (a) CONUS, (b) SE, and (c) QIC regions. Red curves are for solar, blue for wind, and green dashed curves are for the W50%+S50% mix of wind and solar.

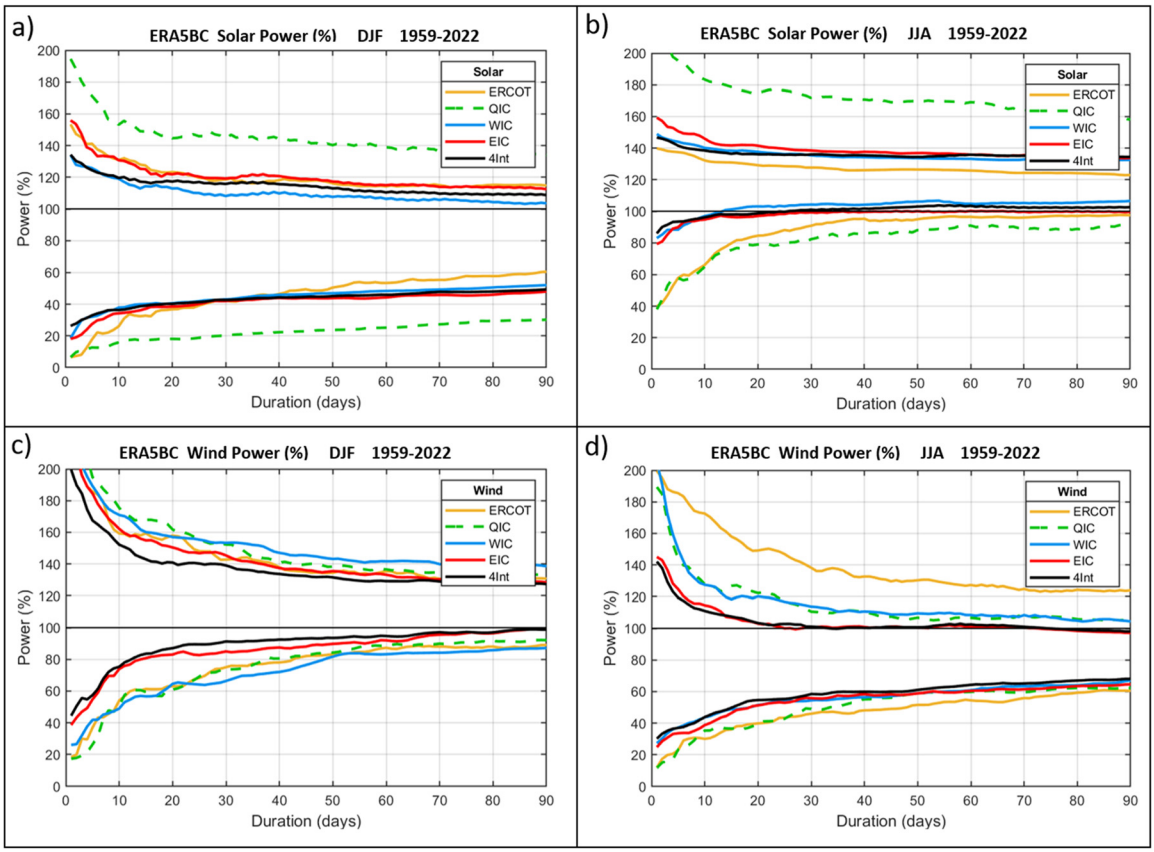

FIG. 16. Intensity–duration diagrams of the largest and smallest normalized power values in the 64-year analysis period, for (a) solar in winter (DJF), (b) solar in summer (JJA), (c) wind in DJF, and (d) wind in JJA. Color-coded lines are for the four interconnect regions (ERCOT, QIC, WIC, EIC, and for the 4Int combination of all four interconnects).

for durations greater than 10 days, winter wind droughts [Fig. 16(c)] for ERCOT and QIC being equal to those for WIC, and ERCOT summer solar floods [Fig. 16(b)] having smaller intensities than all of the other interconnects. These exceptions indicate that geographic variations in drought and flood characteristics can be more important than the size of the region.

Comparing wind and solar droughts in the respective low points of the wind and solar annual cycle variation, solar droughts in winter [Fig. 16(a)] are more intense than wind droughts in summer [Fig. 16(d)]. In contrast, in the high points of the wind and solar annual cycle variation, solar droughts in summer [Fig. 16(b)] are less intense than wind droughts in winter [Fig. 16(c)]. The overall most intense energy droughts are solar droughts in winter.

Next, comparisons are made of all of the non-interconnect regions, NENG, NE, NY, SE, MW, GP, SW, CA, NW, as well as the CONUS (Fig. 17), where the I-D curves for each region are color-coded to match those used in the region map [Fig. 1(b)], with warm colors for the eastern regions and cool colors for the western regions. Of these regions, NENG, NY, and CA are significantly smaller than the rest, and therefore might always be expected to have more intense droughts and floods, but that is not the case, as regional variations again can be larger. Overall, the dominant feature in each of the panels in the figure is the significant spread that exists among the regions, demonstrating the highly regional nature of wind and solar drought characteristics. A second important feature is that in three of the four panels [Figs. 17(a), 17(b), and 17(d)] droughts in the eastern regions are more intense than those in the western regions. The exception to this is that wind droughts in winter [Fig. 17(c)] are most intense in the three western regions (CA, NW, SW).

The focus of this analysis principally has been on wind and solar droughts. However, extreme flood events can also impact grid operations and result in curtailment costs. At short durations, wind flood events tend to be more extreme than solar. For several of these regions in either winter or summer, the normalized wind power at 1 day duration can be very large, e.g., SE 412%; CA 392%; NE 363%; and NY 340% of the long-term mean generation, and even at 30 days duration can exceed 160% (NENG, NE, NY, SE, NW, and CA) [Fig. 17(c)].

An additional aspect of the regional nature of the energy droughts investigated here are the connections between drought occurrences in the subregions and those in the corresponding interconnect regions in which they are embedded. In the supplementary material, we investigate the degree of synchronicity between droughts in the sub-regions and their corresponding larger interconnects, and the extent to which strong transmission links to the larger interconnect could mitigate the specific worst droughts in the sub-regions.

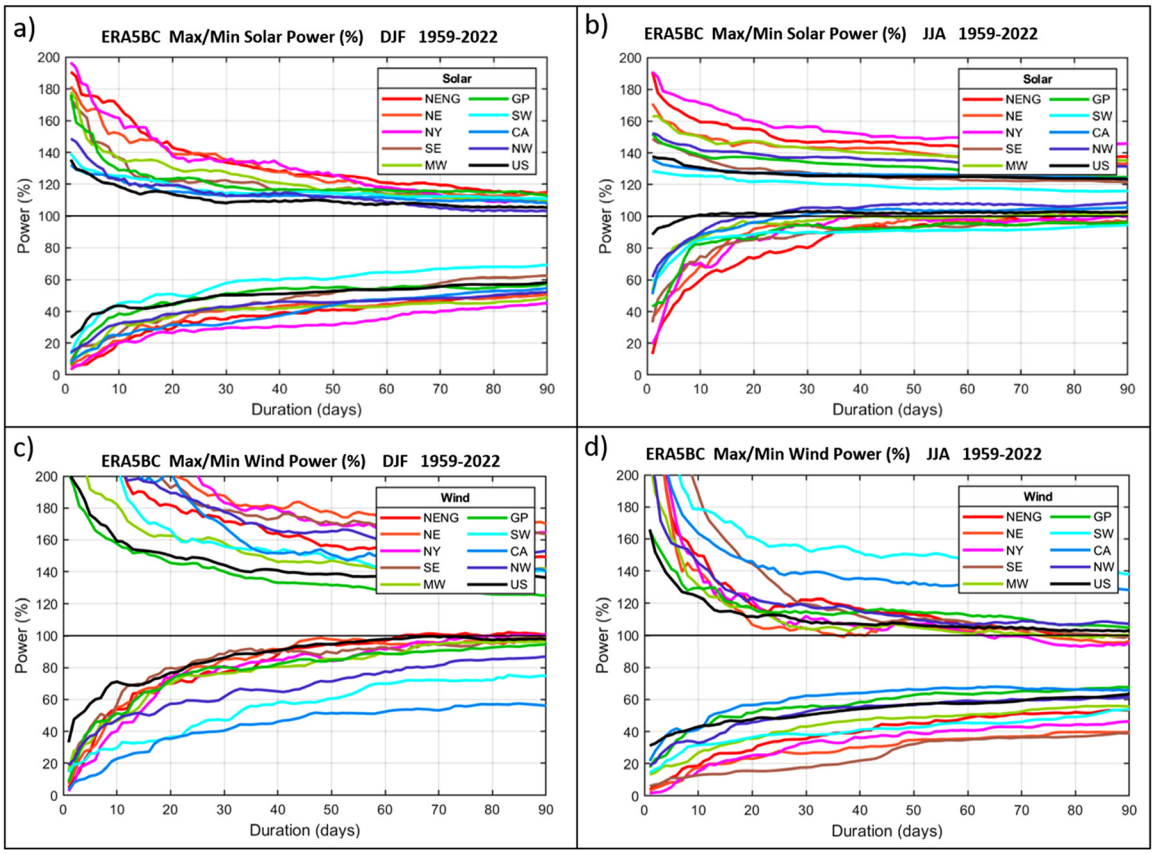

FIG. 17. As in Fig. 16 except for nine subregions plus the CONUS.

IX. DROUGHT-TEMPERATURE DEPENDENCE, COMPARISON TO LOAD VARIATIONS

One additional meteorological relationship of interest is the correlation between wind or solar droughts with temperature. Because electricity demand is highly dependent on temperature,[39] wind and solar droughts that occur during extremely hot or cold periods will be of more consequence than those that occur on temperate days. Figure 18 shows scatter plots of normalized power for the W50%+S50% scenario vs 2 m temperature (taken from the ERA5 reanalysis), for NY and the CONUS regions, for both daily averages and after applying 10 and 30 day running means. The correlation of power and 2m temperature is weak, and fortunately for both of these regions, and for all of the regions investigated, neither the coldest nor hottest days coincide with the worst drought events. Instead, both the NY and CONUS regions' most intense droughts at all durations occur when the region mean daily temperature is approximately 0 °C. For NY, the worst W50%+S50% 1-day droughts, which occur near 0 °C, produce about 12% of the annual average mean generation, while at 10-days duration the worst droughts generation level reaches about 35% of the annual average mean, and at 30-days duration the worst generation level is 60%. For the CONUS region the levels are higher, with the worst 1-day droughts, which also occur near 0 °C, producing about 40% of the annual average mean, while the worst 10-day droughts reach 60%, and the worst 30-day droughts 70%. If as heat pumps become more common, and future loads increase during cold temperatures to the point that at 0 °C they are larger than the long-term mean load, then that increase in load will exacerbate the impact of these worst wind droughts on balancing the energy system.

For temperatures colder than 0 °C, the normalized power increases with decreasing temperature. For the NY region, examining generation characteristics at the far cold tail of the temperature distribution, for 1, 10, and 30 day temperatures colder than −15, −10, and −5 °C, respectively, the minimum generation levels are greater than 30%, 60%, and 70%, all considerably larger than the minimum values near 0 °C of 12%, 35%, and 60%. For the CONUS, the minimum generation also increases with decreasing temperature, such that for 1, 10, and 30 day temperatures colder than −10, −7, and −5 °C respectively, the minimum generation levels are greater than 60%, 75%, and 90%, all considerably larger than the minimum values near 0 °C of 40%, 55%, and 70%. In addition to purely meteorological causal factors, this increase in power with decreasing temperature occurs in part because solar panels are more efficient as temperature decreases. For temperatures greater than 0 °C the normalized power also increases. When the time-mean NY temperatures are 25 °C, the worst 1, 10, and 30 day droughts have generation at 70% and 80% and 90% of the long-term

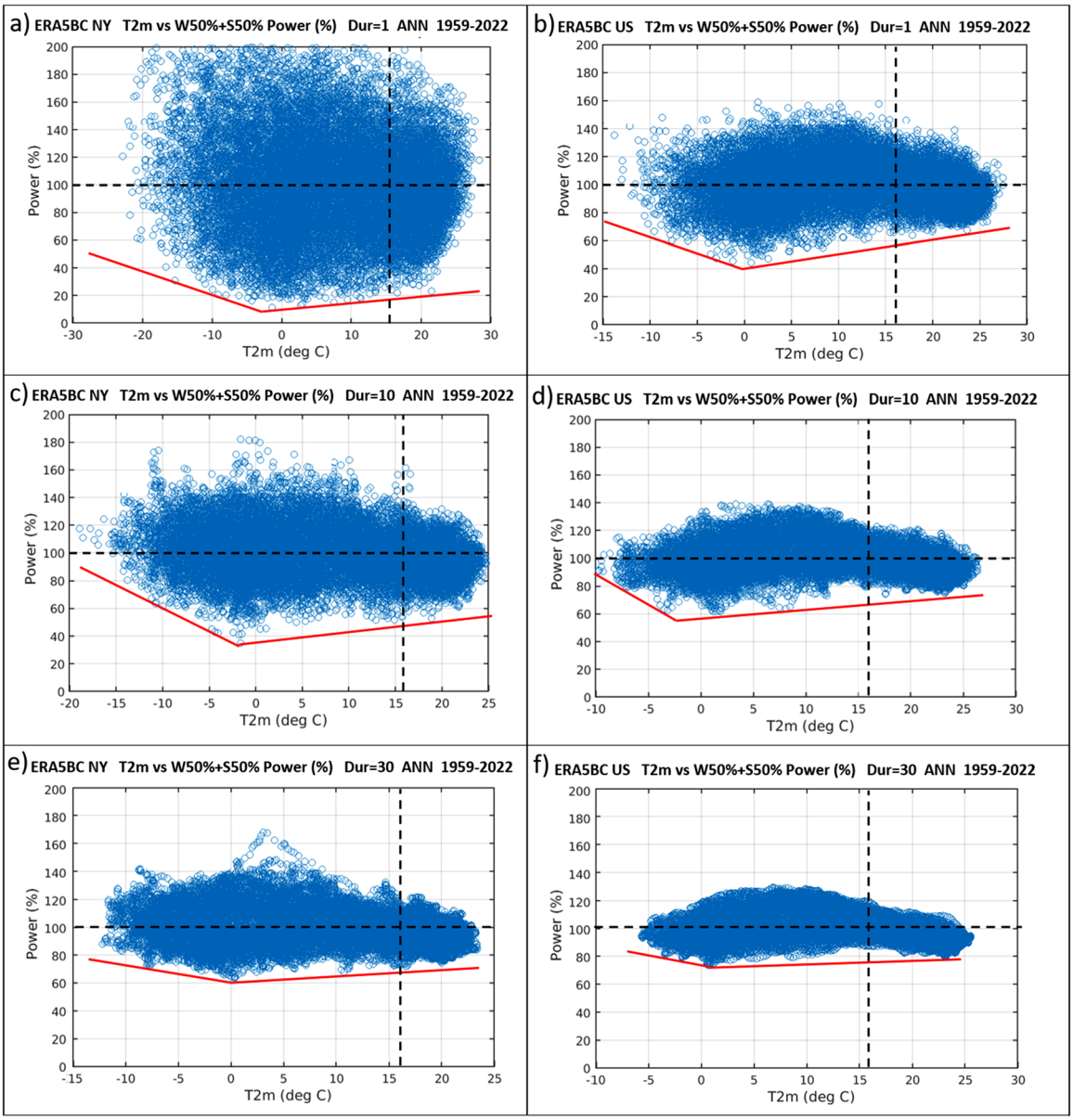

FIG. 18. Scatter plots of normalized power for the W50%+S50% mix of wind and solar vs 2 m temperature, for the NY region with durations of (a) 1 day, (c) 10 days, (e) 30 days, and for the CONUS region with durations of (b) 1 day, (d) 10 days, (f) 30 days. The red lines indicate a lower boundary of the smallest normalized power values. The horizontal dashed line at 100% indicates power generation equal to the long-term mean generation, and the vertical dashed line indicates the temperature (16 °C) at which minimum electricity demand typically occurs.

mean, all again much higher than the minimum generation near 0 °C, although still less than the long-term mean generation.

The trends with temperature shown for the NY and CONUS regions are common to most of the other regions, although the temperature at which the minimum generation occurs can shift depending on whether the region's annual mean temperature is colder or warmer. For example, at 10-days duration, the northwest region [Fig. 19(a)] has its minimum generation near −2 °C, while the southeast region [Fig. 19(b)] has its minimum generation near +15 °C. The SE region then has minimum generation levels that are fairly similar up to 25 °C.

Heating and cooling degree days are traditionally calculated relative to a baseline of approximately 18 °C (65 F) at which temperature-dependent load is at its minimum. Auffhammer *et al.*[39] however finds that based on actual load data that minimum loads occur at somewhat lower temperatures, dependent on the regional power system analyzed. Using a minimum load baseline temperature value of 16 °C, the overall

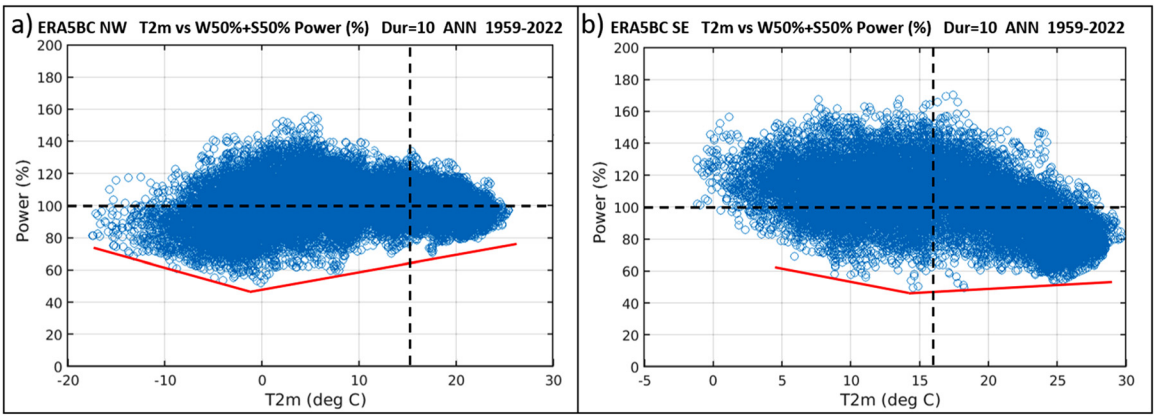

FIG. 19. As in Fig. 18 except for (a) the NW and (b) SE regions for 10-day duration droughts.

dependence of the W50%+S50% generation on temperature indicates that for the NY and CONUS regions (Fig. 18) and for the NW [Fig. 19(a)], balancing energy supply and demand in a renewables-based energy system will be more difficult in winter than in summer, assuming all heating is done with heat pumps that have similar efficiency as air conditioners. That is, the droughts are more extreme for temperatures colder than 16 °C than they are for warmer temperatures, and they occur at temperature values further from the 16 °C baseline. This result is found to hold for all regions analyzed, with the exception of the SE, where balancing supply and demand will be slightly more difficult for warmer temperatures than colder [Fig. 19(b)]. Finally, we note that because often there are relatively few extreme drought events that are coincident with cold or hot temperatures (Figs. 18 and 19), that long multi-decadal data records are needed to make accurate assessments of their impacts.

X. SUMMARY AND DISCUSSION

Bias-corrected values of daily wind and solar power generation derived from the ERA5 meteorological reanalysis (termed ERA5BC) for the period 1959–2022 have been used to investigate the characteristics of wind and solar energy droughts across the contiguous U.S. and most of Canada. Solar power is calculated for fixed-tilt panels with tilt angles that maximize annual energy production. Wind power is calculated at a height of 100 m above ground level, and offshore wind power is accounted for by including three over-water coastal grid points extending to ∼75 km offshore, including the Great Lakes. The overall analysis domain has been divided into regions that correspond to four major North American grid interconnects. Additional regions over which droughts are analyzed include the contiguous U.S. and nine sub-regions within the U.S. that approximately correspond to economic zones (ISOs, TSOs, regional power pools) over which electricity is routinely traded. When assessing droughts over a region, all ERA5BC grid points within that region are weighted equally. Because the energy system has no natural storage, equivalent to soil moisture or snow pack for hydrologic droughts, wind and solar energy droughts are impactful on short time scales, and droughts with durations from 1 to 90 days are analyzed. Droughts are defined as periods of low power generation relative to the long-term mean generation, for wind, solar, or a mix of wind and solar in which each provides 50% of the total mean energy produced. This definition includes the seasonal variations of wind and solar generation, as those variations cannot be ignored when balancing the electric grid. The analysis is presented using mean capacity factors and normalized power, where the normalized power is the ratio of a daily mean CF divided by the long-term mean CF, expressed as a percent.

The main findings are:

- Domain-averaged wind and solar power trends are small compared to the overall variability, decreasing by 2.3% and 1.7% respectively over the 1959–2022 analysis period. Geographic variations of the 64-year trends are greater for wind than for solar, but still small enough that they will not materially affect the calculation of wind and solar energy drought intensities for short to moderate duration droughts.
- Wind and solar power generation are negatively correlated at daily timescales over most of the analysis domain, with the exception of the southwest U. S. Correlation coefficients increase in magnitude for longer timescales as short-term weather variability is filtered out. Correlations are as large as -0.6 in the eastern and far western U.S. and Canada at 30-day timescales. The negative correlations of wind and solar power mean that at most locations in the analysis domain wind and solar power are complementary, providing a significant benefit in reducing the variability of renewable energy generation.
- Although histograms of wind and solar are non-Gaussian, the difference between the mean and median power values for the regions analyzed is typically a few percent, and never larger than 15%. Histograms of a mix of 50% wind and 50% solar on an energy basis are closer to Gaussian, with smaller differences between mean and median. Defining droughts using a percent of the mean or a percent of the median approach would therefore give similar results.
- For small regions such as NY, NENG, NE, and GP, the most intense 1-day wind or solar droughts have normalized power generation less than 5% of the long-term mean generation. For these regions, a solar-only system or a wind-only system with no multi-day storage and no inter-region transmission would require overbuilding capacity by factors of 10× or more to bring generation up to its long-term mean. Only for very large regions

with strong long-distance transmission does overbuilding a solar-only system or a wind-only system with no multi-day storage or import of electricity become conceivably tractable.
- The wind resource in the Great Plains and Texas regions is sufficiently good that over-weighting wind capacity in those areas would help mitigate CONUS scale wind droughts for all duration lengths. The solar resource is sufficiently good in the southwestern U.S. region that overweighting solar capacity in that area would help mitigate CONUS scale solar droughts of durations 10 days and longer. In both cases, this would require that there exist means (either transmission lines or pipelines to carry power-to-gas that is created locally) to export that power to other regions.
- Intensity–duration curves for the most intense droughts present in the 64-year record demonstrate that droughts tend to be more intense for smaller regions (i.e., grid balancing areas), but that large regional variability also exists.
- A regional analysis of wind and solar drought intensities for winter and summer seasons shows that droughts in the eastern regions tend to have greater intensities than those in western regions, with the exception of wind droughts in winter, which are worse in western regions.
- The magnitude of the potential errors that could occur in capacity expansion models using short meteorological datasets of several year's length is demonstrated for the CONUS W50%+S50% scenario. For drought durations of 10–15 days, a return period of 4 years overestimates the minimum generation by 25% compared to a return period of 65 years, while the amount of storage required to fill in the deficits for the two return periods differs by up to 37%.
- Droughts for the W50%+S50% scenario are weakly correlated with 2 m temperature. Minimum power generation occurs for moderately cold temperatures of approximately 0 °C for the NY and CONUS regions for all durations. For most regions and durations, below average generation can occur during the most extreme cold and hot temperatures, indicating that increased load and decreased generation can occur simultaneously. For a renewables-based fully electrified energy system, in all regions except the southeast U.S., winter W50%+S50% droughts will present greater challenges for balancing the electric grid than in summer.

In conclusion, this study has presented an analysis of the characteristics of wind and solar energy droughts, and has provided some insights into how those droughts may impact the optimal design and operation of a future energy system that is highly dependent on renewable generation sources.

SUPPLEMENTARY MATERIAL

See the supplementary material provides an analysis of the degree of synchronicity between droughts in the sub-regions and their corresponding larger interconnects, and the extent to which strong transmission links to the larger interconnect could mitigate the specific worst droughts in the sub-regions.

ACKNOWLEDGMENTS

The authors thank Cathy Smith and two anonymous reviewers.

This work was funded by the NOAA Physical Sciences Laboratory and the NOAA Atmospheric Science for Renewable Energy program. This work was also supported in part by the NOAA cooperative Agreement NA22OAR4320151.

AUTHOR DECLARATIONS

Conflict of Interest

The authors have no conflicts to disclose.

Author Contributions

James M. Wilczak: Conceptualization (lead); Data curation (equal); Formal analysis (lead); Funding acquisition (lead); Investigation (lead); Methodology (lead); Project administration (lead); Resources (lead); Software (equal); Supervision (lead); Validation (lead); Visualization (lead); Writing – original draft (lead); Writing – review & editing (equal). **Elena Akish:** Data curation (equal); Formal analysis (equal); Methodology (equal); Software (equal); Visualization (equal); Writing – review & editing (equal). **Antonietta Capotondi:** Conceptualization (supporting); Formal analysis (supporting); Methodology (supporting); Writing – review & editing (equal). **Gilbert P. Compo:** Conceptualization (supporting); Formal analysis (supporting); Methodology (supporting); Writing – review & editing (equal). **Andrew Hoell:** Conceptualization (supporting); Formal analysis (supporting); Methodology (supporting); Writing – review & editing (equal).

DATA AVAILABILITY

The data that support the findings of this study are available from the corresponding author upon reasonable request.

REFERENCES

[1]J. M. Wilczak, E. Akish, A. Capotondi, and G. P. Compo, "Evaluation and bias correction of the ERA5 reanalysis over the United States for wind and solar energy applications," Energies **17**(7), 1667 (2024).
[2]A. E. MacDonald, C. T. M. Clack, A. Alexander, A. Dunbar, J. Wilczak, and Y. F. Xie, "Future cost-competitive electricity systems and their impact on US CO emissions," Nat. Clim. Change **6**(5), 526–531 (2016).
[3]See https://www.osti.gov/servlets/purl/1257264 for "Eastern Renewable Generation Integration Study: Redefining What's Possible for Renewable Energy" (USDOE, National Renewable Energy Lab. (NREL), Golden, CO); accessed 2016-06-14.
[4]G. Brinkman, D. Bain, G. Buster *et al.*, see https://www.osti.gov/biblio/1804701 for "The North American Renewable Integration Study (NARIS): A U.S. Perspective" (2021).
[5]A. Phadke, U. Paliwal, N. Abhyankar, T. McNair, B. Paulos, D. Wooley, and R. O'Connell, "The 2035 report: Plummeting solar, wind, and battery costs can accelerate our clean electricity future," Technical Report (University of California Berkeley, 2020); available at http://www.2035report.com/wp-content/uploads/2020/06/2035-Report.pdf.
[6]P. Brown and A. Botterud, "The value of inter-regional coordination and transmission in decarbonizing the US electricity system," Joule **5**(1), 115–134 (2021).
[7]D. Raynaud, B. Hingray, B. François, and J. D. Creutin, "Energy droughts from variable renewable energy sources in European climates," Renewable Energy **125**, 578–589 (2018).
[8]P. Patlakas, G. Galanis, D. Diamantis, and G. Kallos, "Low wind speed events: Persistence and frequency," Wind Energy **20**(6), 1033–1047 (2017).
[9]D. J. Cannon, D. J. Brayshaw, J. Methven, P. J. Coker, and D. Lenaghan, "Using reanalysis data to quantify extreme wind power generation statistics: A 33 year case study in Great Britain," Renewable Energy **75**, 767–778 (2015).

[10]N. Ohlendorf and W.-P. Schill, "Frequency and duration of low-wind-power events in Germany," Environ. Res. Lett. **15**(8), 084045 (2020).
[11]B. Li, S. Basu, S. J. Watson, and H. W. J. Russchenberg, "A brief climatology of Dunkelflaute events over and surrounding the North and Baltic Sea areas," Energies **14**(20), 6508 (2021).
[12]P. Potisomporn and C. R. Vogel, "Spatial and temporal variability characteristics of offshore wind energy in the United Kingdom," Wind Energy **25**(3), 537–552 (2021).
[13]M. J. Mayer, B. Biró, B. Szücs, and A. Aszódi, "Probabilistic modeling of future electricity systems with high renewable energy penetration using machine learning," Appl. Energy **336**, 120801 (2023).
[14]F. Mockert, C. M. Grams, T. Brown, and F. Neumann, "Meteorological conditions during periods of low wind speed and insolation in Germany: The role of weather regimes," Meteorol. Appl. **30**(4), e2141 (2023).
[15]F. Liu, X. Wang, F. Sun, and H. Wang, "Wind resource droughts in China," Environ. Res. Lett. **18**(9), 094015 (2023).
[16]P. Potisomporn, T. A. A. Adcock, and C. R. Vogel, "Extreme value analysis of wind droughts in Great Britain," Renewable Energy **221**, 119847 (2024).
[17]J. Jurasz, J. Mikulik, P. B. Dąbek, M. Guezgouz, and B. Kaźmierczak, "Complementarity and 'Resource Droughts' of solar and wind energy in Poland: An ERA5-based analysis," Energies **14**(4), 1118 (2021).
[18]N. Otero, O. Martius, S. Allen, H. Bloomfield, and B. Schaefli, "Characterizing renewable energy compound events across Europe using a logistic regression-based approach," Meteorol. Appl. **29**(5), e2089 (2022).
[19]J. Hu, V. Koning, T. Bosshard *et al.*, "Implications of a Paris-proof scenario for future supply of weather-dependent variable renewable energy in Europe," Adv. Appl. Energy. **10**, 100134 (2023).
[20]J. Kapica, J. Jurasz, F. A. Canales *et al.*, "The potential impact of climate change on European renewable energy droughts," Renewable Sustainable Energy Rev. **189**, 114011 (2024).
[21]A. Gangopadhyay, A. K. Seshadri, N. J. Sparks, and R. Toumi, "The role of wind-solar hybrid plants in mitigating renewable energy-droughts," Renewable Energy **194**, 926–937 (2022).
[22]P. Potisomporn, T. A. A. Adcock, and C. R. Vogel, "Evaluating ERA5 reanalysis predictions of low wind speed events around the UK," Energy Rep. **10**, 4781–4790 (2023).
[23]S. Abdelaziz, S. N. Sparrow, W. Hua, and D. C. H. Wallom, "Assessing long-term future climate change impacts on extreme low wind events for offshore wind turbines in the UK exclusive economic zone," Appl. Energy **354**, 122218 (2024).
[24]C. Gutiérrez, M. Molina, M. Ortega, N. López-Franca, and E. Sánchez, "Low-wind climatology (1979–2018) over Europe from ERA5 reanalysis," Clim. Dyn. **62**, 4155–4170 (2024).
[25]C. Breyer, D. Bogdanov, M. Ram *et al.*, "Reflecting the energy transition from a European perspective and in the global context—Relevance of solar photovoltaics benchmarking two ambitious scenarios," Prog. Photovoltaics **31**(12), 1369–1395 (2022).
[26]S. Allen and N. Otero, "Standardised indices to monitor energy droughts," Renewable Energy **217**, 119206 (2023).
[27]C. Bracken, N. Voisin, C. D. Burleyson, A. M. Campbell, Z. J. Hou, and D. Broman, "Standardized benchmark of historical compound wind and solar energy droughts across the Continental United States," Renewable Energy **220**, 119550 (2024).
[28]B. François, H. D. Puspitarini, E. Volpi, and M. Borga, "Statistical analysis of electricity supply deficits from renewable energy sources across an Alpine transect," Renewable Energy **201**, 1200–1212 (2022).
[29]P. T. Brown, D. J. Farnham, and K. Caldeira, "Meteorology and climatology of historical weekly wind and solar power resource droughts over western North America in ERA5," SN Appl. Sci. **3**(10), 814 (2021).
[30]K. Z. Rinaldi, J. A. Dowling, T. H. Ruggles, K. Caldeira, and N. S. Lewis, "Wind and solar resource droughts in California highlight the benefits of long-term storage and integration with the western interconnect," Environ. Sci. Technol. **55**(9), 6214–6226 (2021).
[31]M. Ohba, Y. Kanno, and D. Nohara, "Climatology of dark doldrums in Japan," Renewable Sustainable Energy Rev. **155**, 111927 (2022).
[32]P. G. Leahy and E. J. McKeogh, "Persistence of low wind speed conditions and implications for wind power variability," Wind Energy **16**(4), 575–586 (2012).
[33]O. Ruhnau and S. Qvist, "Storage requirements in a 100% renewable electricity system: Extreme events and inter-annual variability," Environ. Res. Lett. **17**(4), 044018 (2022).
[34]H. Hersbach, B. Bell, P. Berrisford *et al.*, "The ERA5 global reanalysis," Q. J. R. Meteorol. Soc. **146**(730), 1999–2049 (2020).
[35]S. L. Barnes, "Mesoscale objective map analysis using weighted time-series observations," NOAA Technical Memorandum No. ERL NSSL; 62 (1973).
[36]C. Draxl, A. Clifton, B. M. Hodge, and J. McCaa, "The wind integration national dataset (WIND) toolkit," Appl. Energy **151**, 355–366 (2015).
[37]J. Wohland, D. Brayshaw, and S. Pfenninger, "Mitigating a century of European renewable variability with transmission and informed siting," Environ. Res. Lett. **16**(6), 064026. (2021).
[38]M. J. Hayes, *Drought Indices* (Van Nostrand's Scientific Encyclopedia, 2006).
[39]M. Auffhammer, P. Baylis, and C. Hausman, "Climate change is projected to have severe impacts on the frequency and intensity of peak electricity demand across the United States," Proc. Natl. Acad. Sci. **114**(8), 6 (2017).